JAERI-M
83-029

# EVALUATION REPORT ON CCTF CORE-I REFLOOD TEST CI-19 (RUN 38) — EXPERIMENTAL ASSESSMENT OF THE EVALUATION MODEL FOR THE SAFETY ANALYSIS ON THE REFLOOD PHASE OF A PWR-LOCA —

February 1983

Yoshio MURAO, Kazuo FUJIKI and Hajime AKIMOTO

日本原子力研究所
Japan Atomic Energy Research Institute

JAERI-Mレポートは，日本原子力研究所が不定期に公刊している研究報告書です。
入手の問合わせは，日本原子力研究所技術情報部情報資料課（〒319-11茨城県那珂郡東海村）あて，お申しこしください。なお，このほかに財団法人原子力弘済会資料センター（〒319-11 茨城県那珂郡東海村日本原子力研究所内）で複写による実費頒布をおこなっております。

JAERI-M reports are issued irregularly.
Inquiries about availability of the reports should be addressed to Information Section, Division of Technical Information, Japan Atomic Energy Research Institute, Tokai-mura, Naka-gun, Ibaraki-ken 319-11, Japan.



編集兼発行　日本原子力研究所
印　　刷　いばらき印刷㈱

JAERI-M 83-029

# Evaluation Report on CCTF Core-I Reflood Test C1-19 (RUN 38)

## - Experimental Assessment of the Evaluation Model for the safety analysis on the reflood phase of a PWR-LOCA -

Yoshio MURAO, Kazuo FUJIKI+ and Hajime AKIMOTO

Division of Nuclear Safety Research,
Tokai Research Establishment, JAERI

(Received January 29, 1983)

A test named the Evaluation Model (EM) test was performed, whose test conditions were simulated the reflood phase predicted with the safety evaluation analysis. The test results were compared with the blindfold results predicted by Evaluation Model (EM) codes. The main conclusions are as follows:

(1) The core heat transfer model built in the EM codes gives conservative results.

(2) The system models in the present EM codes are found to be well balanced integrally over the system.

(3) Conservative items and items to be improved are pointed out.

The downcomer slow water accumulation observed in the lower flow rate test was not appeared in the EM test.

Keywords: Reactor Safety, REflood Experiment, Hydrodynamics, Safety Analysis Code, Heat Transfer, PWR, LOCA

---

The work was performed under Contract with the Atomic Energy Bureau of Science and Technology of Japan.

+) Division of Nuclear Safety Evaluation, Tokai Research Establishment, JAERI.

JAERI－M 83 － 029

# 大型再冠水円筒第一次炉心試験Ｃ１－19（Run 38）評価報告書
## ―PWR－LOCA時再冠水過程の安全解析用評価モデルの実験的評価―

日本原子力研究所東海研究所安全工学部
村尾　良夫・藤木　和男[+]・秋本　肇

（1983年1月29日受理）

評価モデル（EM）試験と名付けた試験を行った。その試験条件は，安全評価解析で計算された再冠水過程を模擬したものである。試験結果を伏せて評価モデル（EM）コードにより計算を行い，試験結果と計算結果との比較を行った。主な結論は次の通りである。

(1) EM コードに組込まれた炉心熱伝達モデルは保守的な結果を与える。

(2) 現在のEM コードの中のシステムモデルは，システム全体としてよく均衡のとれたものである。

(3) 保守的な事柄および改良すべき事柄を指摘できた。

低流量試験で見い出されたダウンカマ蓄水率の低下は，本試験では現われなかった。

---

本報告書は，電源開発促進対策特別会計施行令に基づき，科学技術庁からの委託によって行った研究の成果である。

+）安全解析部

Contents

# 目　　次

List of tables



List of figures

## I. Introduction

In order to assess the evaluation model for the safety analysis in a Pressurized Water Reactor (PWR) during the reflood phase of a loss-of-coolant accident (LOCA), a test named the Evaluation Model (EM) test, C1-19 (Run 38), was performed by using the Cylindrical Core Test Facility (CCTF).

The CCTF is one of the facilities of the Large Scale Reflood Test Program which has been initiated since April 1976, and built in the reflood test program under the three lateral cooperation among U.S., FRG and Japan, named 2D/3D Project.

The objectives of the Large Scale Reflood Test Program are:

(1) Demonstration of the safety margin in the current safety evaluation analysis on the effectiveness of the Emergency Core Cooling System (ECCS) during the refill and reflood phases of a PWR-LOCA.

(2) Provision of information for analytical modeling of thermo-hydrodynamic phenomena during the refill and reflood phases of a PWR LOCA.

(3) Verification of an integral reflood analysis code, "REFLA", and a US-developed reactor transient analysis code, "TRAC".

For this program, the Slab Core Test Facility (SCTF) was also constructed to investigate the two-dimensional thermo-hydrodynamic behavior in the core and the upper plenum. Both facilities are used to achieve the above mentioned task.

In the test, the initial and the boundary conditions were determined based on the results of the safety evaluation calculations. In parallel with the test, pre-test calculations were made with Evaluation Model (EM) codes, WREM and WRAP, in Japan and U.S., respectively.

In the present study, the effect of the Emergency Core Cooling (ECC) flow rate on the downcomer water accumulation will be additionally discussed. The slow water accumulation observed in the previous test[1] was attributed to the too conservative ECC flow rate. In this test, the ECC flow rate was taken based on the EM calculation and higher than the previous test. Therefore, the effect will be expected to be examined.

The results of the WRAP prediction was partly used for the EM code assessment, for lack of information.

The main results of CCTF test C1-19 (Run 38) are shown in Appendix.

## II. Experiment

### 1. Apparatus

The CCTF was designed to reasonably simulate the flow conditions in the primary system of a 4-loop PWR during the refill and reflood phases of a LOCA. The reference reactors are the Trojan reactor and, in certain aspects, the Ohi reactor in Japan. The vertical dimensions and the length of the flow pathes of the system components are kept as close to the reference reactors as possible. The each flow area of the system component is scaled down in proportion to the scaling factor, 1/21.4, of the core flow area. The primary loop consists of three intact loops and a broken loop.

Each loop has an active steam generator, a loop seal section, a pump simulator, and an ECC injection port. An ECC injection system consists of the accumulator (Acc injection into the lower plenum, the ACC injections into the cold legs and the low pressure coolant injection (LPCI) into the cold legs.

Figure 1 shows the vertical cross section of the pressure vessel. The left side is the CCTF and the right side is the typical PWR. In order to provide a wider downcomer, the volume of the core baffle of the PWR was included in the volume of the downcomer in the scaling of the CCTF downcomer. The core baffle has a flow path from the lower plenum to the upper plenum and relatively high flow resistance devices, for equalizing the pressure drop to that in the core, resulting in the slow water accumulation in the core baffle. When the same amount of water enters in the pressure vessel, the vessel having the core baffle introduces more rapid water accumulation in the downcomer, while the vessel having the wider downcomer without the core baffle introduces slower water accumulation in the downcomer. Therefore the CCTF provides more conservatisms in the downcomer water accumulation than the PWR. The wider downcomer is considered to better simulate the hydrodynamic behavior. The initial wall temperature of the vessel wall was adjusted to simulate the heat release from the wall to the unit flow area of the downcomer[1].

The core consists of thirty-two 8 × 8 electrically heated rod bundles and simulates the 15 × 15 array fuel assemblies. The core is subdivided into some power regions. It is possible to control the radial

power distribution. The axial peaking factor is about 1.49. Each bundle consists of 57 heated rods and 7 non-heated rods. The heated rods consists of 12 high, 17 medium and 28 low powered rods with power ratios of 1.1, 1.0, and 0.95, respectively.

The design of the upper plenum internals is based on the old Westinghouse 17 × 17 array fuel assemblies. The internals consist of 12 control rod guide tubes, 4 support columns, 8 stub mixers, 2 orifice plates and 6 open holes. The radial dimensions of each internal is scaled down by factor of 8/15 from that of an actual reactor.

The steam generators are of the U-tube and shell type. The tube length is about 15 m and about 5 m shorter than that of an actual reactor however, it is enough to simulate the heat transfer between the secondary to primary side[2]. The secondary side is filled with high pressure saturated water. The pump simulators are equipped with orifice plates to simulate the flow resistance and with vanes to simulate counter-current flow limited (CCFL) characteristics of an actual pump.

The containment vessel is simulated with two tanks, i.e. Containment tanks 1 and 2. The former is used for the water collector vessel and is equipped with a steam water separator and a liquid level meter to measure the discharge rate of the water overflowing from the broken cold leg nozzle. The latter is used for the simulated containment vessel. However, a large volume tank is necessary to represent a scaled containment volume. Therefore, the purpose of this tank is to maintain a constant back pressure by means of a pressure control system. Thus, the pressure-time behavior of the PWR containment vessel during a LOCA is not simulated. Containment tank 1 with the steam water separator is connected to the broken cold leg nozzle and Containment tank 2 is connected to the broken cold leg and to Containment tank 1. The steam in Containment tank 2 is exhausted to the atmosphere through the pressure control valve. In this facility, the break was assumed to be at the outer surface of the biological shield. A section of cold leg piping about 2.8 m long is connected to the broken cold leg nozzle and the fluid is discharged into the Containment tank 1 through a pipe of double size.

## 2. Instrumentation

Many differential pressure transducers and thermocouples were

installed to measure the differential pressures, fluid temperatures and wall temperatures. In the places where the velocity of liquid phase is very low, the frictional loss and the acceleration loss are negligible compared with the gravitational loss. Hence it is considered that the pressure drops expressed in the water head indicate the collapsed water level or the water accumulation in the downcomer, the core, the upper plenum and the lower plenum. The flow meters are equipped to measure the injection flow rates.

The pitot tubes are positioned at the downstream side of the exit of the steam generators. About 900 thermocouples are uniformly attached on the clad surface of the simulated core in order to determine whether the thermo-hydrodynamic behavior in the core is one-dimensional or not. Sheathed thermocouples of 0.5 mm diameter are burried on the outside clad surface. Including other detectors, more than 1600 channel of data were recorded.

## 3. Test procedure

The test procedures were as follows: After establishing the initial conditions of the test, the lower plenum was filled with saturated water to a specified level of 0.9 m for this test. Electric power was applied to the heater rods of the core. When the maximum temperature reached the specified temperature, the water in the Accumulator was injected into the Lower Plenum (Acc/LP mode). When the water was estimated to reach the bottom of the core i.e. at the time of the Bottom Of Core RECovery (BOCREC), decay of the heating power was scheduled to be automatically started at a programmed rate, corresponding to the reactor decay heat. After the assumed time delay, the injection location was changed from the lower plenum to the ECC ports of the three intact cold legs. The ECC water was still supplied from the accumulator and this period is defined as the Accumulator mode (Acc mode). After a specified time delay, the injection mode was transferred from the accumulator injection mode (Acc mode) to the Low Pressure Coolant Injection (LPCI) mode (LPCI mode). The system pressure of the Containment tank 2 was kept constant. The test conditions of this test are listed in Table 1. The power was supplied to 3 radially divided power zones of the core and the ratio of the power supplied to a rod of three zones was 1.286, 1.10 and 0.837.

## III. Evaluation Model Calculations

### 1. WREM calculation in JAERI

Simulating the LOCA-ECCS audit calculations[5] performed at JAERI, the same WREM code was used and the similar noding for the system calculation was adopted. The clad ballooning and rupture model, and the flow blockage model were not used for heated rods.

#### System model

The RELA4-FLOOD EM reflood model was used for the system calculation. The schematic of the system nodalization is shown in Fig. 2. Three intact loops were expressed by an equivalent single intact loop. The heat slabs corresponding to the vessel internals and pipe walls were not considered. The model consists of 23 control volumes, 25 junctions and 26 heat slabs. The core is represented by single control volume including 12 heat slabs. The volume corresponding to the space between the top of the heated core and the upper core support plate was included in the core volume. For the heat slabs of the core, the structure of the heated rods was considered, however, the boron nitride, BN, was substituted for the magnesia, MgO, used as the insulator in the upper and lower portion of the rods. In the steam generators, the primary and secondary sides were represented with two and one control volumes for each loop, respectively.

The junctions 31 and 32 were specially used for the broken cold keg nozzle and the connected pipe as recommended in the RELAP4-FLOOD code manual[3]. This model is called the two-pipe model in this study. The flow resistance of the nozzle has been tuned to the base case test[1]. The ECC injection line was modeled with the junctions 34 and 35 and they were assumed to be connected to the downcomer.

The carry-over rate fraction, i.e. the ratio of the core outlet mass flow rate to the core inlet mass flow rate, was evaluated with the correlation developed by Babcock and Wilcox (B & W) Company. Natural convective heat transfer correlation was applied to the secondary surface of the steam generator heat slabs. The occurrence of choking was forbidden for the all junctions including the break junctions.

According to the restriction of the equilibrium assumption in

RELAP4, the temperatures of the injected ECC water were rised to nearly saturated values, i.e. 392K, to prevent strong condensation at the injected place. The core inlet subcooling requested for the FLECHT correlation of the core heat transfer was set to 64K, assuming that the lower plenum fluid temperature was the average of the ECC water temperature and the well-mixed lower plenum water temperature at the Bottom of Core Recovery (BOCREC).

Fuel pin model

The TOODEE2 single heated rod model was used for the pre-reflood heat-up and reflood temperature transient analysis of the highest powered rod. The center portion of the rod was devided into 10 three inches long heat slabs in the same manner as the EM analysis for the rupture and oxidization of the fuel rod cladding. The heat capacity tables for fuel rods were replaced with those for the heated rods. The gap size was set to be very small value, i.e. $2.54 \times 10^{-5}$ m. The multiplication factors of the region I, II and III of the FLECHT heat transfer coefficient correlation were set to 0.85, 0.95 and 0.85, respectively.

## 2. WRAP calculation in U.S.

The WRAP[6] code was used for the prediction. The model and the nodalization were similar to the WREM calculation. The different points are as follows:

1) The LPCI injection point was the node of the code leg.
2) In the downcomer, a heat slab was considered, however, an complete phase separation model was used. Therefore, this model gives no voiding even the boiling occures in the downcomer.
3) A different carry-over rate fraction correlation was used.
4) A different core inlet subcooling, i.e. 49K was used for the FLECHT correlation. The value was the well-mixed fluid temperature in the lower plenum at the BOCREC.

## IV. Results and Discussion

### 1. Momentum and mass balance over the system

#### Core flooding rate

The core flooding rate has been thought to be one of the most sensitive parameters for the core heat transfer as well as the core inlet temperature and the pressure in the core since the FLECHT tests[4]. Since the core flooding rate is governed by the thermo-hydrodynamic behaviors over the system, the comparison of the measured core flooding rate with the predicted is useful for the assessment of the overall system model in the EM codes. Figure 3 shows the core flooding rates estimated in the CCTF test and the predicted with the WREM and the WRAP. The WREM and WRAP predict the core flooding rate well after 139 and 119 seconds, respectively. The estimated core flooding rate was obtained from the mass balance calculation as described in Appendix C. Because of the smoothing procedure in the calculation, the estimated core flooding rate in the early transient before about 132 seconds (about 30 seconds after flood) does not have enough accuracy to discuss the agreement between the estimated and the predicted. However, it is found that the predicted flooding rate is lower than the estimated on the time average and has conservative value. When the core flooding rates become lower than 1 in/s, a steam cooling correlation is requested to be used for the core heat transfer above the quench front in the safety evaluation criteria.

The core flooding rate become less than 1 in/s at 170 seconds in the CCTF test and the WRAP prediction and at 145 seconds in the WREM prediction. However, the flooding rates estimated and predicted with WREM and WRAP agree well with each other after 170 seconds.

From the above discussion, it can be concluded that the present model is well balanced integrally over the system and predicts the flooding rate conservatively in early transient and accurately in later period.

#### Mass and momentum balance

Since the flooding rate might be influenced by many factors in the integral test, it is very important to analyze the reason why the EM

codes predict the core flooding rate well.

The core flooding rate, $\dot{m}_F$, can be expressed as follows[1],

$$\dot{m}_F = \dot{m}_C + \dot{m}_U + \sum_{i=1}^{3} \dot{m}_{Ii} + \dot{m}_B \quad , \tag{1}$$

$$\dot{m}_I = \sqrt{2\Delta P_I \rho_I / K_I} \quad , \tag{2}$$

$$\dot{m}_B = \sqrt{2\Delta P_B \rho_B / K_B} \quad , \tag{3}$$

$$\Delta P_I = \Delta P_D - \Delta P_C - \Delta P_U \quad , \tag{4}$$

$$\Delta P_B = \Delta P_I + \Delta P_{BCN} \quad , \tag{5}$$

where $\dot{m}$ is the mass accumulation rate or the mass flow rate, $\Delta P$ is the differential pressure, $\rho$ is the fluid density, K is the so-called K factor and subscripts C, U, I, B, D and BCN denote the core, the upper plenum, the intact loop, the broken loop, the downcomer and the broken cold leg nozzle and its connecting pipe, respectively.

The Eq. (5) describing the effect of the pressure drop at the broken cold leg nozzle has been easily derived from the thought that the pressure in the pressure vessel rises $\Delta P_{BCN}$ more and the pressures at both ends of the inact loops rise $\Delta P_{BCN}$ more, however, the pressure at one end of the broken loop, the pressure in the upper plenum rises $\Delta P_{BCN}$ more and the pressure at another end of broken loop, the pressure of the containment, does not change.

The contribution of each term to the core flooding rate is summarized in Table 2. The WREM code overestimates the water accumulation rate in the core, $\dot{m}_C$, and underestimates the water accumulation rate in the upper plenum, $\dot{m}_U$, and the mass flow rate through the four loops, $\dot{m}_I$s and $\dot{m}_B$, at 100 seconds after flood. The same tendency appears at 200 seconds after flood. These discrepancies cancel with each other and the predicted core flooding rates agree well with the measured flooding rate.

Pressure drop at the broken cold leg nozzle and loop mass flow rates

Figure 4 shows the measured and the predicted pressure drops across the intact and the broken loops, i.e. $\Delta P_I$ and $\Delta P_B$. Since the pressure

drop at the broken cold leg nozzle, $\Delta P_{BCN}$, is equal to ($\Delta P_B$ - $\Delta P_I$) from Eq. (5), the predicted $\Delta P_{BCN}$ can be evaluated as shown in Fig. 4. The measured $P_{BCN}$ is about 2.5 times higher than the predicted with the WREM. According to the WREM code manual, the RELAP4-FLOOD uses the two-pipe model shown in Fig. 5 for the broken cold leg nozzle to avoid the unreasonably large pressure drop at the nozzle. The two-pipe model for the broken cold leg nozzle gives concervative results, i.e. the lower core flooding rate and the lower pressure in the core due to the smaller pressure drop at the nozzle.

Since the lower $\Delta P_{BCN}$ causes the lower pressure in the intact and the broken loops, the underestimation of $\Delta P_{BCN}$ introduces the lower fluid densities, $\rho_I$ and $\rho_B$ in the respective loops. As expressed in Eqs. (2) and (3), this cases the underestimation of the $\dot{m}_I$ and $\dot{m}_B$ in the WREM calculation. As expressed in Eqs. (5) and (3), the underestimation of the pressure drop at the broken cold leg nozzle, $\Delta P_{BCN}$, also causes the underestimation of the $\Delta P_B$ and consequently the underestimation of the $\dot{m}_B$.

Upper plenum water accumulation

Figure 6 shows the measured water accumulation in the upper plenum. In the WREM prediction, the water accumulation model was not used. Since the average water accumulation rate from the 200 seconds to 500 seconds is estimated to be 0.23 kg/s or about 5 % of the core flooding mass flow rate, the neglect of the upper plenum water accumulation introduces only about 5 % lower core flooding rate, i.e. slightly conservative results.

Core water accumulation

Figure 7 shows the measured and the predicted water accumulations in the core and the downcomer. The predicted core collapsed water levels have the tendency to increase at a constant rate, while the measured level in the CCTF test approaches a constant level.

The measured water accumulation rate is higher than the predicted rate in the initial period, however, the measured rate decreases with time. In the WREM, a correlation for the carry-over rate fraction, i.e. B & W correlation, was used and in the WRAP, a different correlation was used.

The measured carry-over rate fraction after 200 seconds is about

0.98, while the predicted with WREM is about 0.8.

The further discussion will be made in the discussion on the core thermo-hydrodynamic behaviors.

Downcomer water accumulation

The collapsed water level in the downcomer is compared with the WREM predictions in Fig. 7. The measured collapsed water level is equal to the overflow level in early period of the transient and become lower than the level after 145 seconds, while the predicted water level is exactly equal to the overflow level. The slow water accumulation observed in the base case test[1] was not appeared in this test. This is thought to be due to higher ECC flow rate of this test, i.e. in the base case test, the ACC water could not fill the downcomer completely and the higher steam flow through the downcomer carried out some amount of LPCI water from the intact cold legs, resulting in the slow water accumulation in the downcomer. However, in this test, the subcooled water was completely filled in the downcomer during the ACC injection period and heated up and boiled in the later period. Further discussion on the downcomer level will be made in the later section.

As derived from Eqs. (1) to (5),

$$\dot{m}_F = \dot{m}_C + \dot{m}_U + \sum_{i=1}^{3} \sqrt{2\Delta P_I \rho_I / K_I} + \sqrt{2(\Delta P_I + P_{BCN})\rho_B / K_B} \qquad (6)$$

where

$$\Delta P_I = \Delta P_D - \Delta P_C - \Delta P_U \quad , \qquad (7)$$

i.e. the higher $(\Delta P_D - \Delta P_C)$ results in the higher $\dot{m}_F$. Therefore the over predicted $(\Delta P_D - \Delta P_C)$ is less conservative than the measured since the higher core flooding rate, $m_F$, induces the higher core cooling capability.

Pressure in the core

Figure 8 shows the measured and the predicted pressures in the core. The higher measured pressure is considered to be introduced by the pressure drop at the broken cold leg nozzle, $\Delta P_{BCN}$.

## 2. Energy balance in the system

### Core inlet fluid temperature

The core inlet fluid temperature measured and calculated with WREM code are shown in Fig. 9. The low subcooling in the calculation is introduced from the input of the calculation, where the ECC water temperature was set to be nearly saturated.

The core inlet subcooling required for the FLECHT correlation built in the WREM was also the input which was independent of the predicted core inlet water temperature. The value of the subcooling, 64K, was determined in the WREM and, 49K, in the WRAP based on the well-mixed water temperature in the lower plenum at the BOCREC. Judging from the Fig. 9, the inputted core inlet fluid subcooling for the FLECHT correlation is too large to produce conservative results of the reflood heat transfer.

### Downcomer and lower plenum

The fluid temperature transients measured in the downcomer are shown in Fig. 10. The location of measuring points are indicated in Fig. 1. The subcooled water filled in the downcomer during the Acc injection period is found to be gradually replaced with the saturated water entering from the intact cold leg nozzle during the LPCI injection period. Because the injected ECC water was heated with the steam flowing through the intact loops and the fluid temperature was saturated in the LPCI period while that was subcooled in the Acc period.

As the subcooled downcomer water entered the core, the subcooled water moved downwards and the saturated water entered the downcomer. The bulk boiling of the saturated water initiated and the subcooled water was heated due to the heat released from the heated downcomer wall. The fluid temperature at the lowest elevation, $T_{D5}$, shows saturation temperature at 165 seconds after flood. If the downcomer wall would not be heated up, it had taken about 30 seconds more for $T_{D5}$ to show the saturation temperature.

When the fluid temperature at the highest elevation, $T_{D1}$, is saturated, the downcomer collapsed water level, $\Delta P_D$, begins to decrease and when $T_{D5}$ is saturated, $\Delta P_D$ approaches the quasi-steady value. This indicates that the reduction of the downcomer head is induced by the

voiding in the downcomer due to the heat release from the downcomer wall (the pressure vessel wall). In the WREM prediction, the downcomer consists of one node without "heat slab" and the nearly saturated ECC water was injected into the downcomer instead of the cold leg. Hence the WREM predicted that the core inlet water temperature was nearly saturated and the collapsed water level in the downcomer was nearly the overflow level.

In the lower plenum, the measured fluid temperature shows high subcooling. This indicates the water in the lower portion of the lower plenum is nearly stagnant and does not mix well with the water from the downcomer. It is thought that this is the reason why the measured core inlet water temperature approaches the saturation temperature in a short time. It is necessary to use at least two nodes for the lower plenum in order to represent the stagnant region and the mixing region in the lower plenum.

Steam generator outlet plenum temperature

Figure 11 shows the measured and the predicted fluid temperature transients at the steam generator outlet plenums. The curves indicate nearly the same superheat and the estimation error of ±20K of the fluid temperature induces the error of ±2.2 % in the loop mass flow rates because of the change of the density. It can be concluded that the steam generator model suitably simulates the observed heat transfer phenomena.

## 3. Core thermo-hydrodynamic behavior

Figure 12 shows the measured and the predicted clad surface temperature histories at the location of the maximum power density. Both EM codes predict similar temperature histories with each other. The predicted temperatures are higher than the measured.

In the system calculation, though the core flooding rate is well estimated, the core inlet water temperature and the pressure in the core are not well estimated. Therefore, it is difficult to identify the model which introduces the conservative results on the clad surface temperature.

In order to evaluate the core heat transfer model, the post-test calculation with the WREM code was preformed giving the measured core boundary conditions. The post-test calculation gives almost the same

tendency as the pre-test predictions. It indicates that the discrepancy of the clad surface temperature is mainly produced by the conservatisms of the core heat transfer model.

Figure 13 shows the measured core collapsed water level, the quench front envelopes and the contour lines of void fractions. If the froth level is defined as the top of the mixture with the averaged void fraction less than 0.9, the froth level reached the top of core within about 14 seconds, i.e. the Acc injection period. This means that considerably large amount of water was accumulated in the core. However, in the FLECHT test referred in the modeling of the EM code, the dispersed flow was observed above the quench front, and the froth level, the top of the two-phase mixture, was roughly identical with the quench front[4]. This is considered to be the reason why poor heat transfer based on the dispersed flow was calculated in the EM codes. Since the poorer heat transfer gives more conservative core cooling than that measured in the EM test, the present core heat transfer model is considered to be acceptable for a EM code.

Since the core water accumulation observed in the EM test is almost identical with those observed in the other CCTF tests, the above mentioned explanation can be applied generally.

The core collapsed water levels predicted with WREM is also shown in Fig. 13. In the test, it is clearly found that the core was filled with two-phase mixture and the quench front was advancing and finally the whole core was quenched in spite of the low core collapsed water level. However in the prediction, the location of the quench front is closely related to the core collapsed water level and the quench of the core above the core collapsed water level is inhibited by the logics in the quench model of the EM code even if the clad surface temperature falls down below the quench temperature.

Therefore, more realistic quench model must be established to remove the inconsistency mentioned above.

## V. Conclusion

A CCTF test named the Evaluation Model (EM) Test was performed. The test conditions simulated the reflood phase predicted with the safety evaluation analysis. The test results were compared with the blindfold results predicted by Evaluation Model (EM) codes. The following conclusions were obtained:

1. The core heat transfer model built in the EM codes gives conservative results. This is caused by the more water accumulation in the CCTF tests than in the FLECHT test referred in the modeling of the EM code.
2. An agreement between the predicted and the estimated core flooding rates were obtained and the agreement shows that the system models in the present EM codes are well balanced integrally over the system.
3. The agreement mentioned above was introduced by cancelling the discrapancy of several factors which influence the core flooding rate.
4. The model for the broken cold leg nozzle, i.e. the two-pipe model and the model for the upper plenum, i.e. no de-entrainment model gives conservative results.
5. The steam generator model gives good results.
6. The measured collapsed water level increased to the overflow level in early period of the transient and decreased gradually, while the predicted water level was exactly equal to the overflow level. The downcomer voiding model must be considered in the EM model.
7. The downcomer slow water accumulation observed in the base case test was not appeared in the EM test. Accordingly, the ECC bypass through the downcomer during the reflood phase is not necessary to consider in the EM calculation.
8. The present quench model, in which the quench propagation is closely correlated with the movement of the collapsed water level in the core, must be improved to express the observed phenomena, i.e. the quench front propagated independently of the movement of the core collapsed water level.
9. The model for the core collapsed water level must be improved to give a conservative or realistic pressure difference between the downcomer and the core head.
10. The water in the lower portion of the lower plenum was almost

stagnant and not mixed well with the water from the downcomer. Therefore, at least two nodes are necessary to represent the stagnant region and the mixing region in the lower plenum.

Nomenclature

$\dot{m}$ : Mass flow rate
$\Delta P$ : Differential pressure
K : K factor ($\equiv \Delta P/\frac{1}{2}\rho v^2$)
P : Pressure
$\rho$ : Density
v : Velocity
T : Fluid temperature

(Subscripts)

C : Core
F : Core flooding
U : Upper plenum
I : Intact loop
B : Broken loop
BCN: Broken cold leg nozzle
D : Downcomer

Acknowledgement

The authors are much indebted to Messrs. T. Sudoh, T. Iguchi, J. Sugimoto and T. Okubo for their technical supports. We would like to express our thanks to Dr. M. Nazawa, Director of Nuclear Safety Research Center, Drs. S. Katsuragi, and M. Ishikawa, Head and Deputy Head of Division of Nuclear Safety Research, respectively, and Dr. K. Hirano, Chief of Reactor Safety Lab. II for their guidance and encouragement for this program. We also would like to express our appreciation to the 2D/3D project members of USA and FRG, especially Dr. L. S. Tong of USNRC and Prof. Dr. F. Mayinger of T. U. München for valuable discussions.

stagnant and not mixed well with the water from the downcomer. Therefore, at least two nodes are necessary to represent the stagnant region and the mixing region in the lower plenum.

Nomenclature

$\dot{m}$ : Mass flow rate
$\Delta P$ : Differential pressure
K : K factor ($\equiv \Delta P / \frac{1}{2} \rho v^2$)
P : Pressure
$\rho$ : Density
v : Velocity
T : Fluid temperature

(Subscripts)

C : Core
F : Core flooding
U : Upper plenum
I : Intact loop
B : Broken loop
BCN: Broken cold leg nozzle
D : Downcomer

Acknowledgement

The authors are much indebted to Messrs. T. Sudoh, T. Iguchi, J. Sugimoto and T. Okubo for their technical supports. We would like to express our thanks to Dr. M. Nazawa, Director of Nuclear Safety Research Center, Drs. S. Katsuragi, and M. Ishikawa, Head and Deputy Head of Division of Nuclear Safety Research, respectively, and Dr. K. Hirano, Chief of Reactor Safety Lab. II for their guidance and encouragement for this program. We also would like to express our appreciation to the 2D/3D project members of USA and FRG, especially Dr. L. S. Tong of USNRC and Prof. Dr. F. Mayinger of T. U. München for valuable discussions.

stagnant and not mixed well with the water from the downcomer. Therefore, at least two nodes are necessary to represent the stagnant region and the mixing region in the lower plenum.

Nomenclature

$\dot{m}$ : Mass flow rate
$\Delta P$ : Differential pressure
K : K factor ($\equiv \Delta P / \frac{1}{2} \rho v^2$)
P : Pressure
$\rho$ : Density
v : Velocity
T : Fluid temperature

(Subscripts)

C : Core
F : Core flooding
U : Upper plenum
I : Intact loop
B : Broken loop
BCN: Broken cold leg nozzle
D : Downcomer

Acknowledgement

The authors are much indebted to Messrs. T. Sudoh, T. Iguchi, J. Sugimoto and T. Okubo for their technical supports. We would like to express our thanks to Dr. M. Nazawa, Director of Nuclear Safety Research Center, Drs. S. Katsuragi, and M. Ishikawa, Head and Deputy Head of Division of Nuclear Safety Research, respectively, and Dr. K. Hirano, Chief of Reactor Safety Lab. II for their guidance and encouragement for this program. We also would like to express our appreciation to the 2D/3D project members of USA and FRG, especially Dr. L. S. Tong of USNRC and Prof. Dr. F. Mayinger of T. U. München for valuable discussions.

References

(1) Murao, Y. et al.: Experimental study of system behavior during reflood phase of PWR-LOCA using CCTF, J. Nucl. Sci. and Technol. 19 [9], pp. 705∿719, (1982).

(2) Waring, J.P. and Hochreiter, L.E.: PWR FLECHT-SET phase B1 evaluation report, WCAP-8583, (1975).

(3) WREM: Water reactor evaluation model Revision 1, NUREG-75/056, (1975).

(4) Lilly, G.P. et al.: PWR FLECHT COSINE LOW FLOODING RATE TEST SERIES evaluation report, WCAP-8838, (1977).

(5) An audit analysis for evaluation of ECCS of Tsuruga Nuclear Power Station Unit 2 (in Japanese), Prepared by JAERI, (1980).

(6) Private communication, Gregory, M.V., Savannah River Laboratory, (1981).

(7) Trojan nuclear plant, Final safety analysis report volume 1 ∿ 9, DOCKET-50344-38 ∿ 46, (1973).

Table 1 Test conditions

| Items | Values | Referred values[1] |
|---|---|---|
| System pressure | 0.2 MPa | 0.2 ∿ 0.26 MPa |
| Initial average linear power | 1.4 KW/m | 1.34 KW/m[2] |
| Initial peak linear power | 2.95 KW/m | 2.95 KW/m |
| Radial peaking factor | 1.286 | 1.435 |
| Axial peaking factor | 1.49 | 1.495 |
| Local peaking factor | 1.1 | 1.027 |
| Total peaking fractor | 2.108 | 2.204 |
| Decay curve of power | ANS × 1.2 + Actinide × 1.1 | ANS×1.2 + Actinide×1.1 + Delayed neutron |
| Maximum initial clad temp. | 1143 k | 1143 k |
| Downcomer wall temp. | 471 k | 443 k[4] |
| Other wall temp. | 392 k | - |
| Steam generator secondaty side water temp. | 538 k | 538 k[3] |
| K factor of primary loop ECC injection conditions | 25 | 24.45[3] |
| ACC flow rate | | |
| from lower plenum | 0.103 $m^3/s$ × 3 sec | 0.105 ∿ 0.0797 $m^3/s$[3] |
| from cold legs | 0.090 $m^3/s$ × 11 sec | |
| ACC water temp. | 308 k | 308 k |
| ACC injection period | 14 sec | 14 sec[3] |
| LPCI flow rate | 1.11 × $10^{-2} m^3/s$ | 1.11 × $10^{-2} m^3/s$[3] |
| LPCI water temp. | 308 k | 308 k |

Note

1) Tsuruga Unit 2[(5)]
2) Trojan[(7)] 2% over power, considered 30 sec afte shutdown with power decay fraction and delayed neutron effect of Tsuruga Units 2.[(5)]
3) Conditions referred in FLECHT-SET tests.[(2)]
4) Equivalent wall temp., see Appendix of Ref.(1).

Table 2 Contribution of individual terms in mass balance to core flooding rate

| | 100 sec after BOCREC* | | | 200 sec after BOCREC* | | |
|---|---|---|---|---|---|---|
| | CCTF | WREM | Discrepancy | CCTF | WREM | Discrepancy |
| $\dot{m}_C$ (kg/s) | 0.57 | 1.23 | -0.66 | 0.29 | 1.04 | -0.75 |
| $\dot{m}_U$ (kg/s) | 0.029 | 0 | +0.029 | 0.20 | 0 | +0.20 |
| $\dot{m}_I$ (kg/s) | 3.54 | 3.31 | +0.23 | 3.41 | 3.04 | +0.37 |
| $\dot{m}_B$** (kg/s) | 1.69 | 1.38 | +0.31 | 1.49 | 1.25 | +0.24 |
| $\dot{m}_F$*** (kg/s) | 5.83 | 5.92 | +0.09 | 5.14 | 5.33 | -0.19 |

* BOCREC occurred at 102 sec.

** Total value of 3 intact loops.

*** $\dot{m}_F = \dot{m}_C + \dot{m}_U + \dot{m}_I + \dot{m}_B$

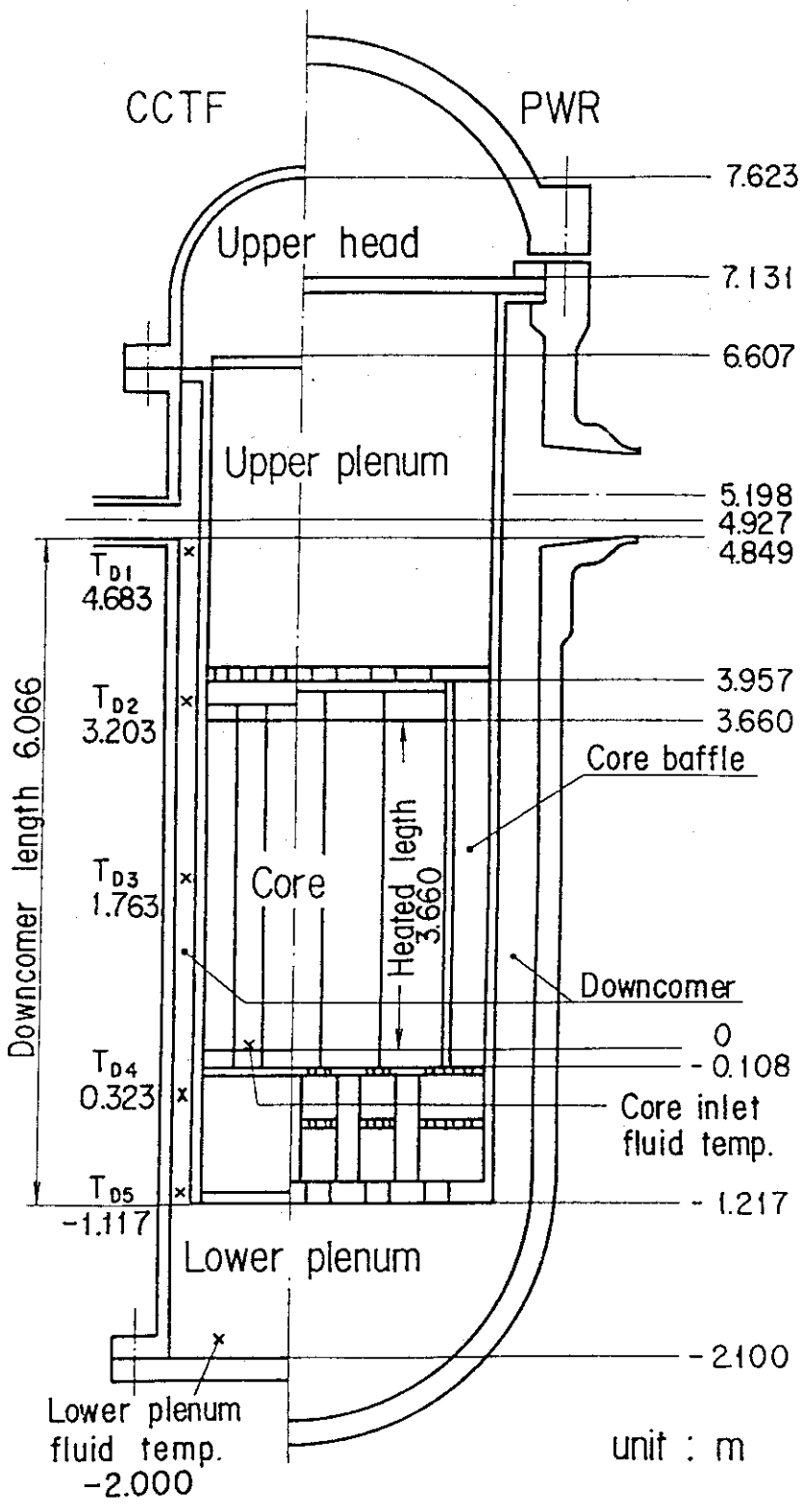


Fig.1 Vertical cross section of pressure vessel

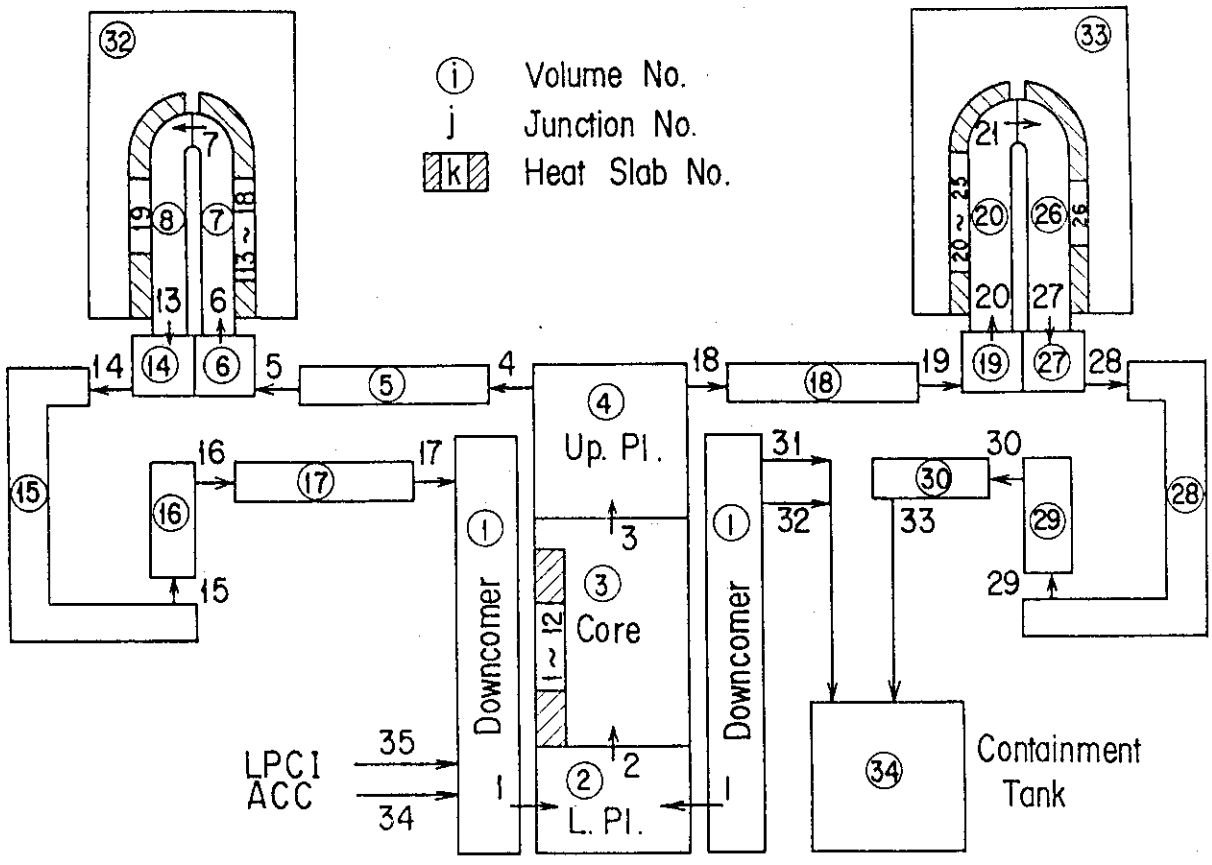


Fig.2 Schematic of system nodalization

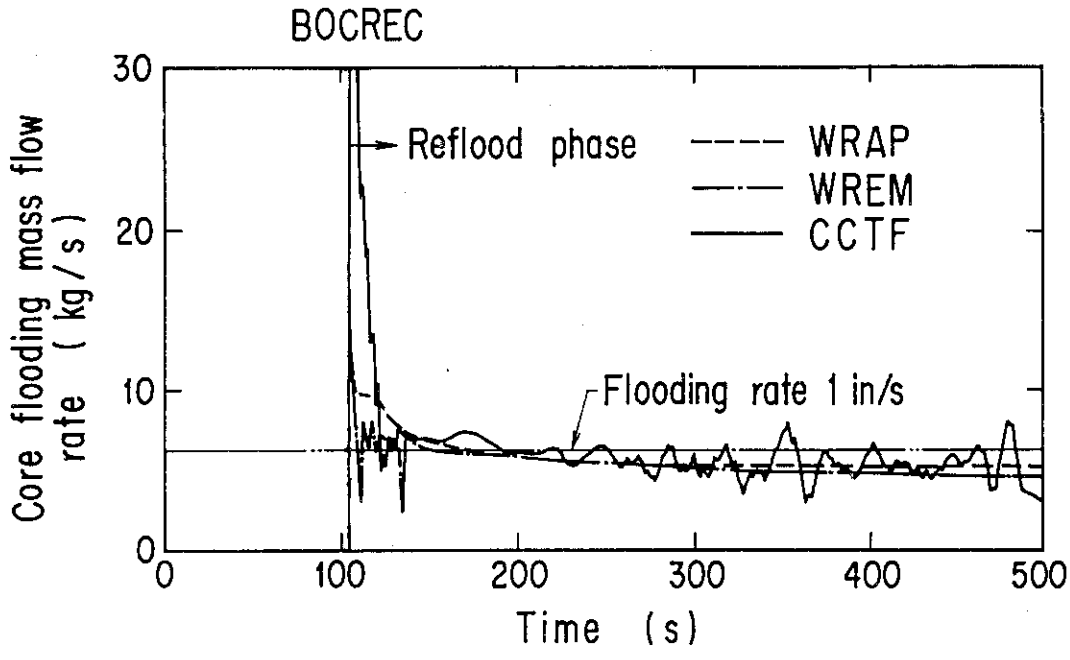


Fig.3 Core flooding rate

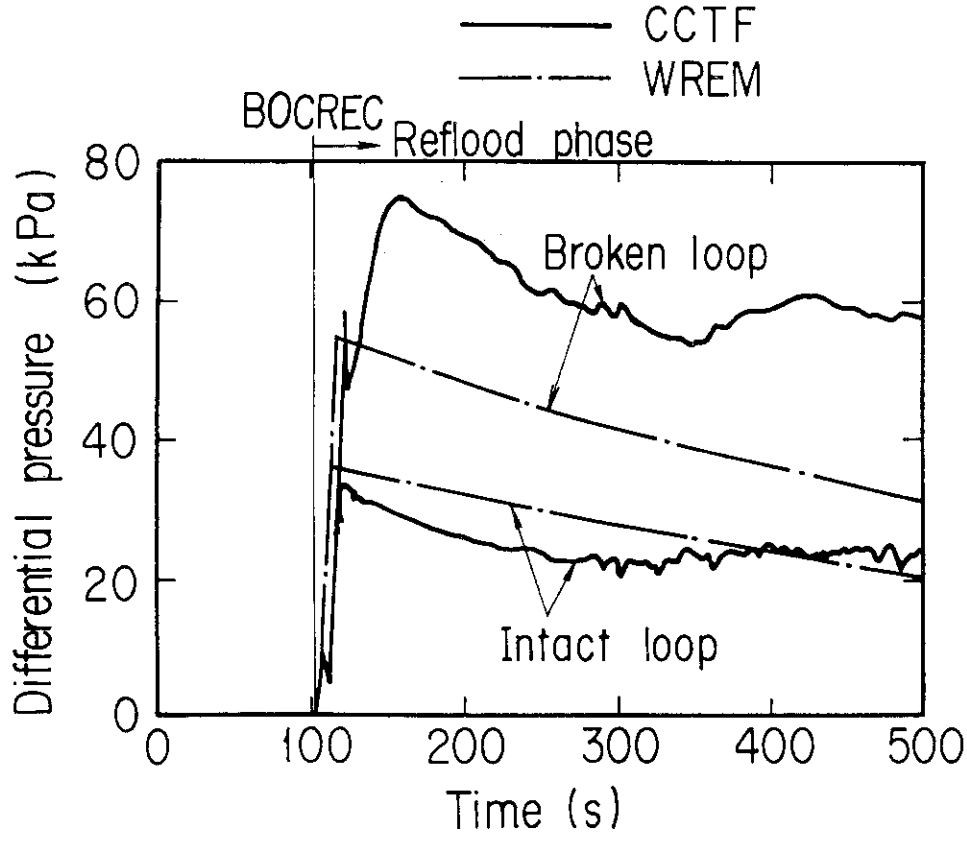


Fig.4 Pressure drop across intact and broken loops

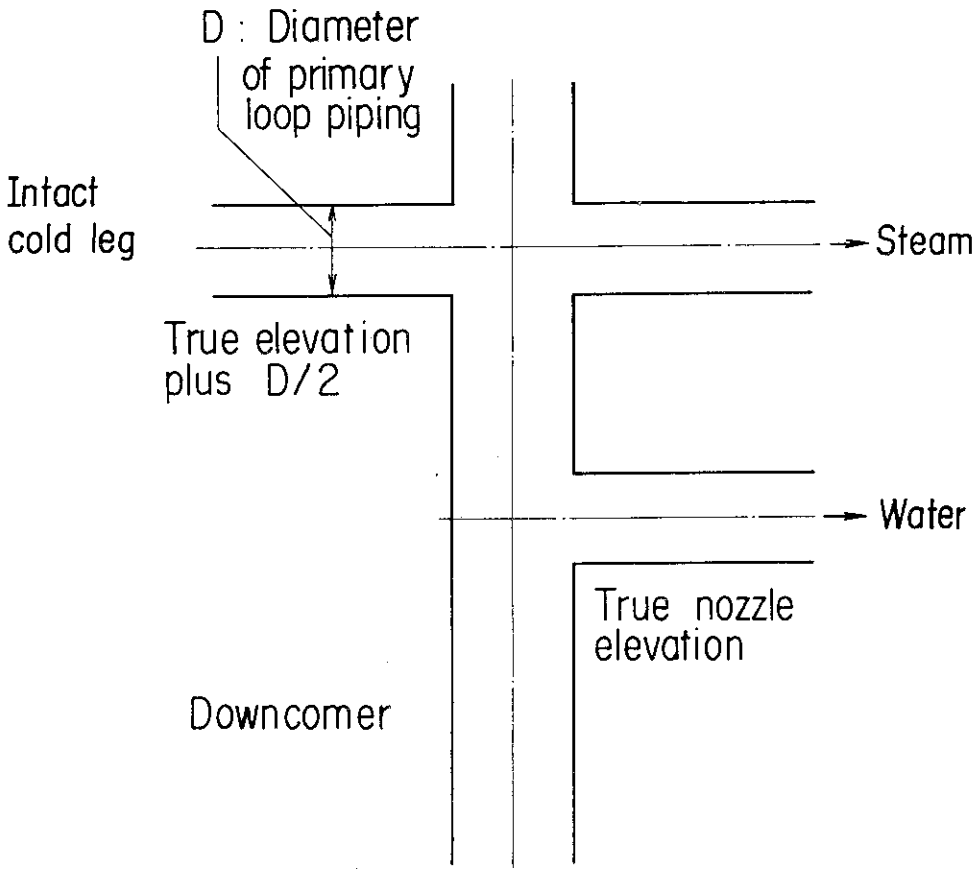


Fig.5 Concept of two-pipe model

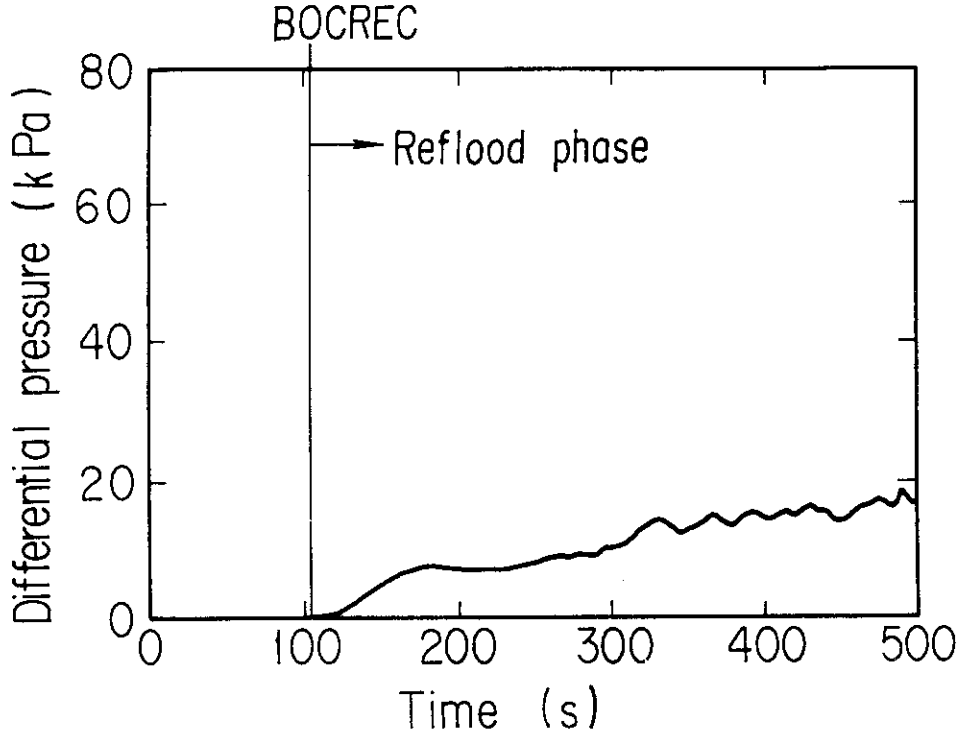


Fig.6 Water accumulation in upper plenum

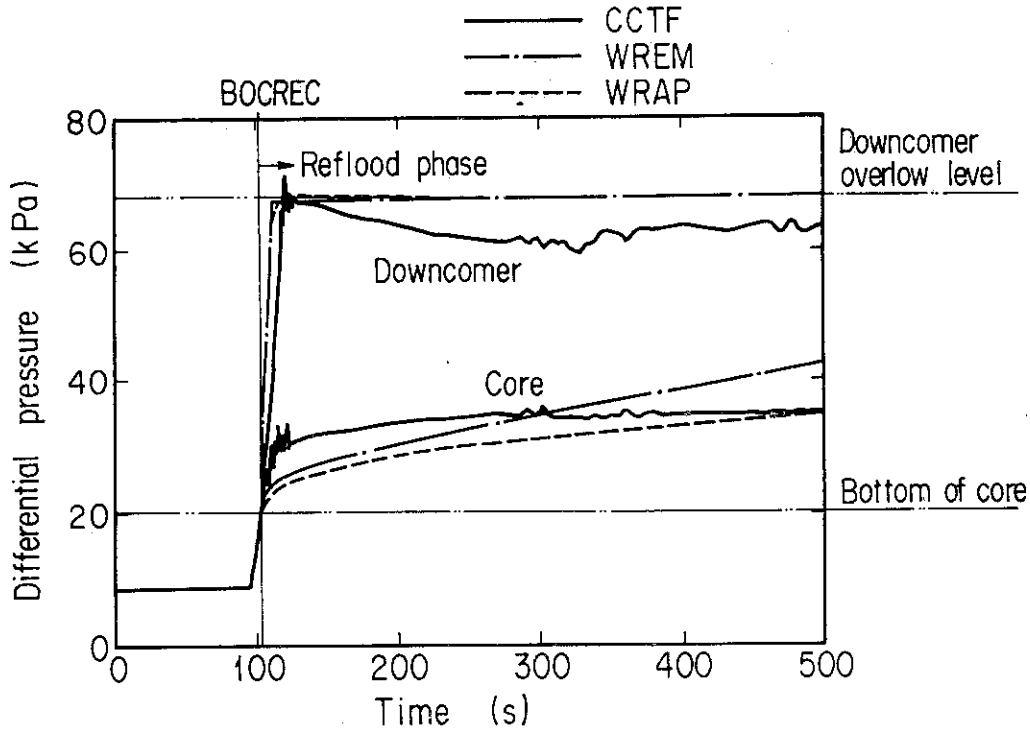


Fig.7 Water accumulation in core and downcomer

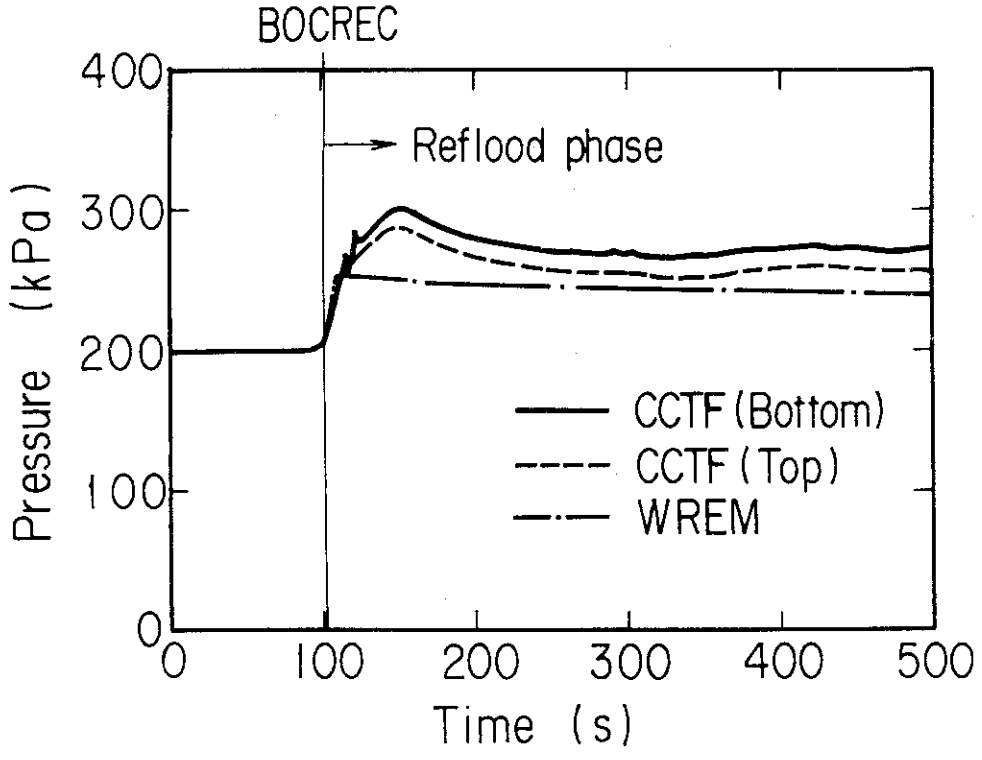


Fig.8 Pressures in core

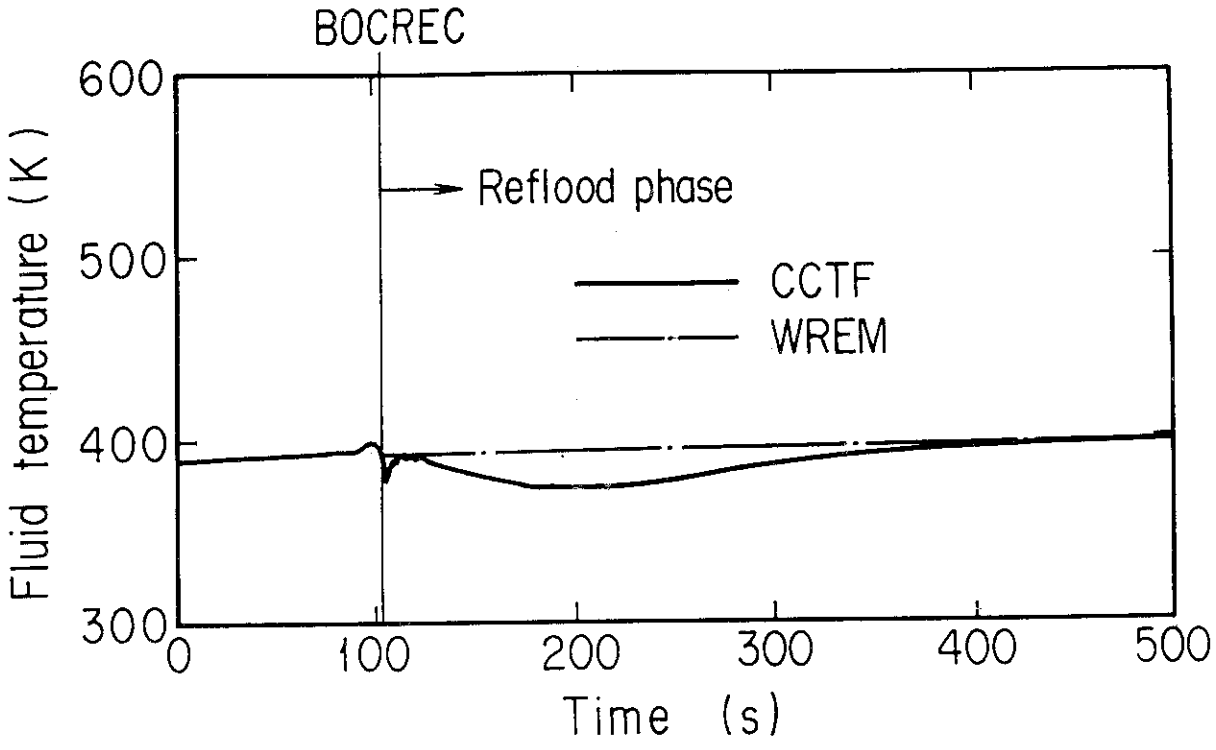


Fig.9 Core inlet fluid temperature

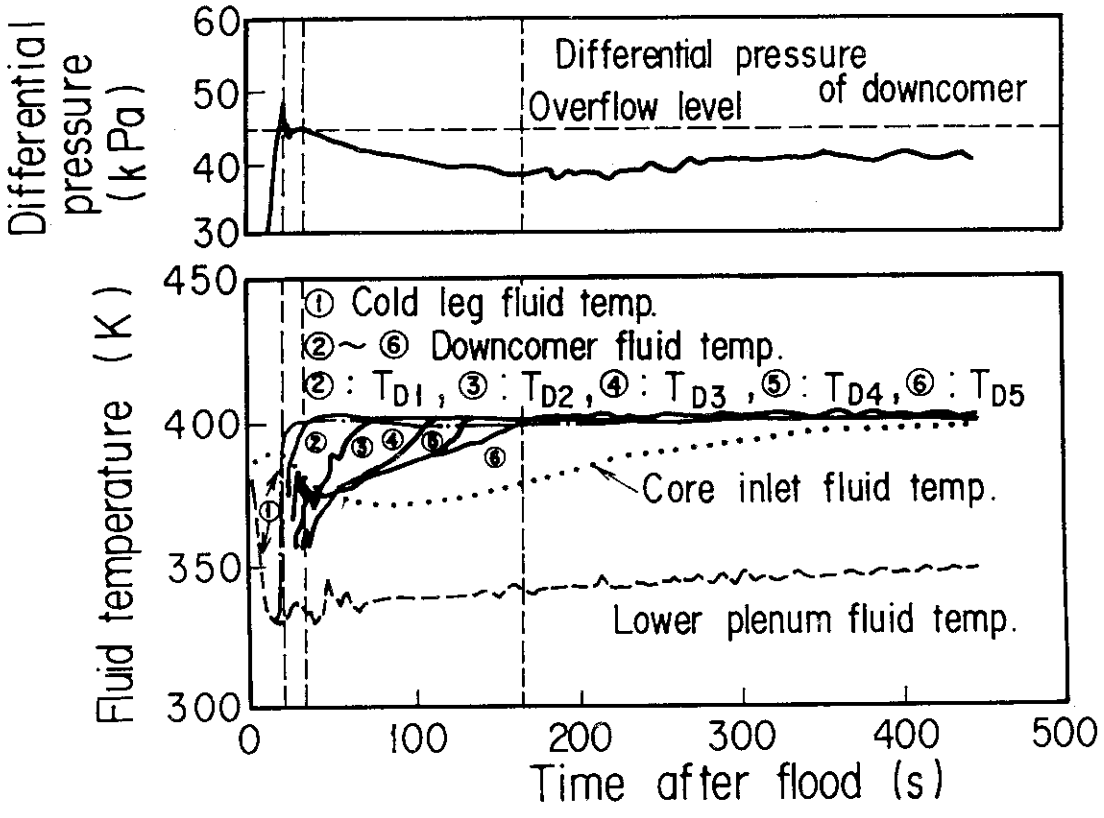


Fig.10 Fluid temperatures in cold leg, downcomer, lower plenum and core inlet and differential pressure of downcomer

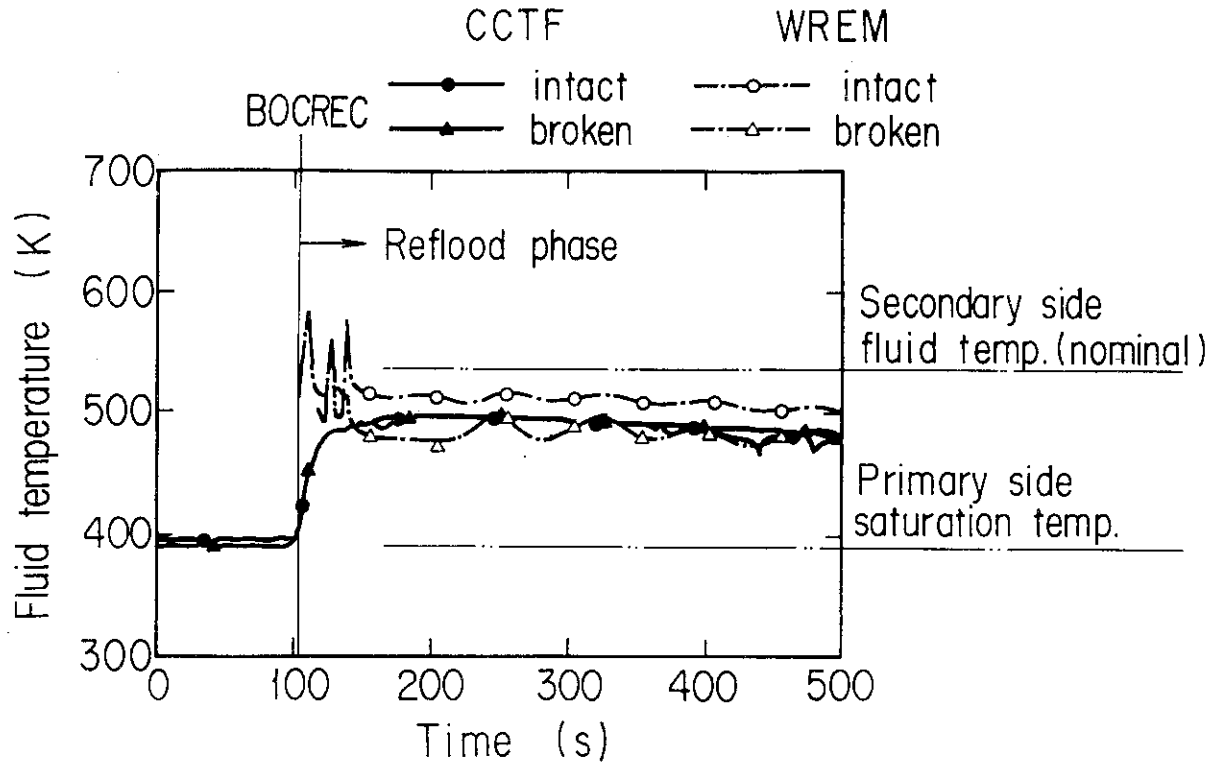


Fig.11 Fluid temperatures at steam generator outlet plenum

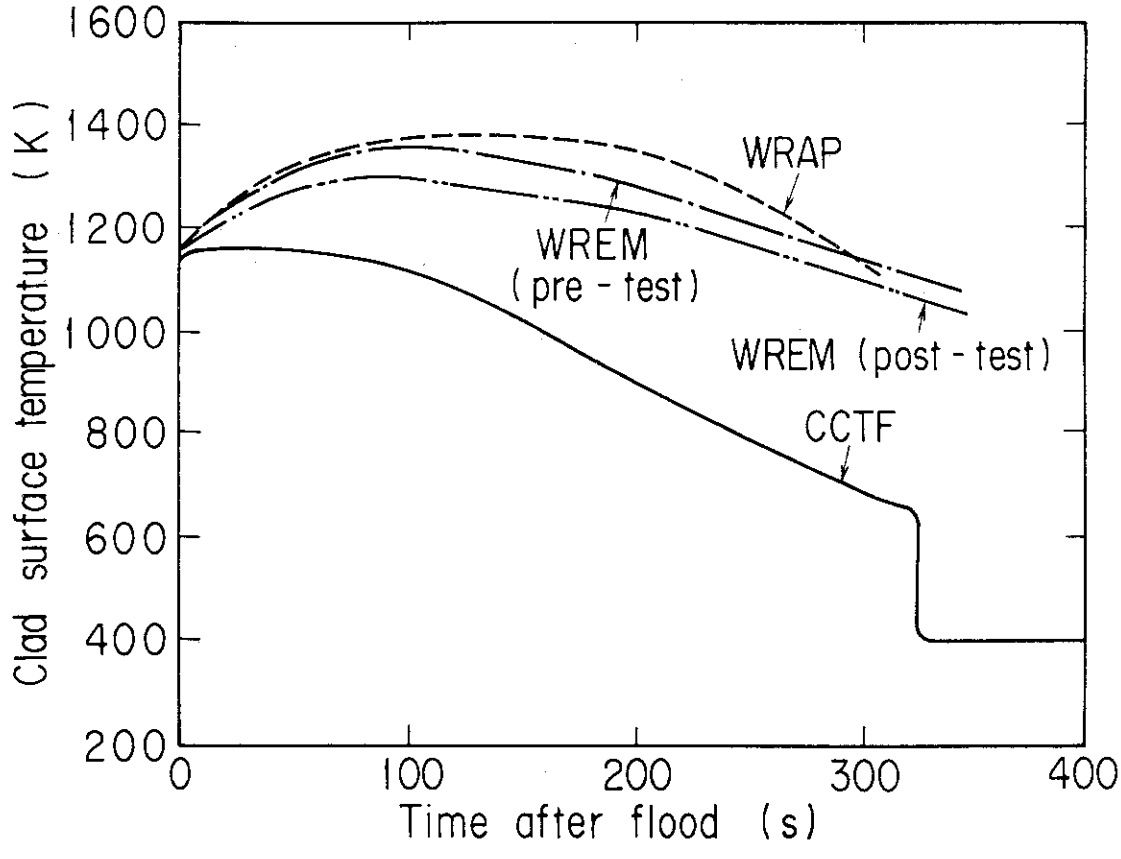


Fig.12 Clad surface temperature at location of maximum power density

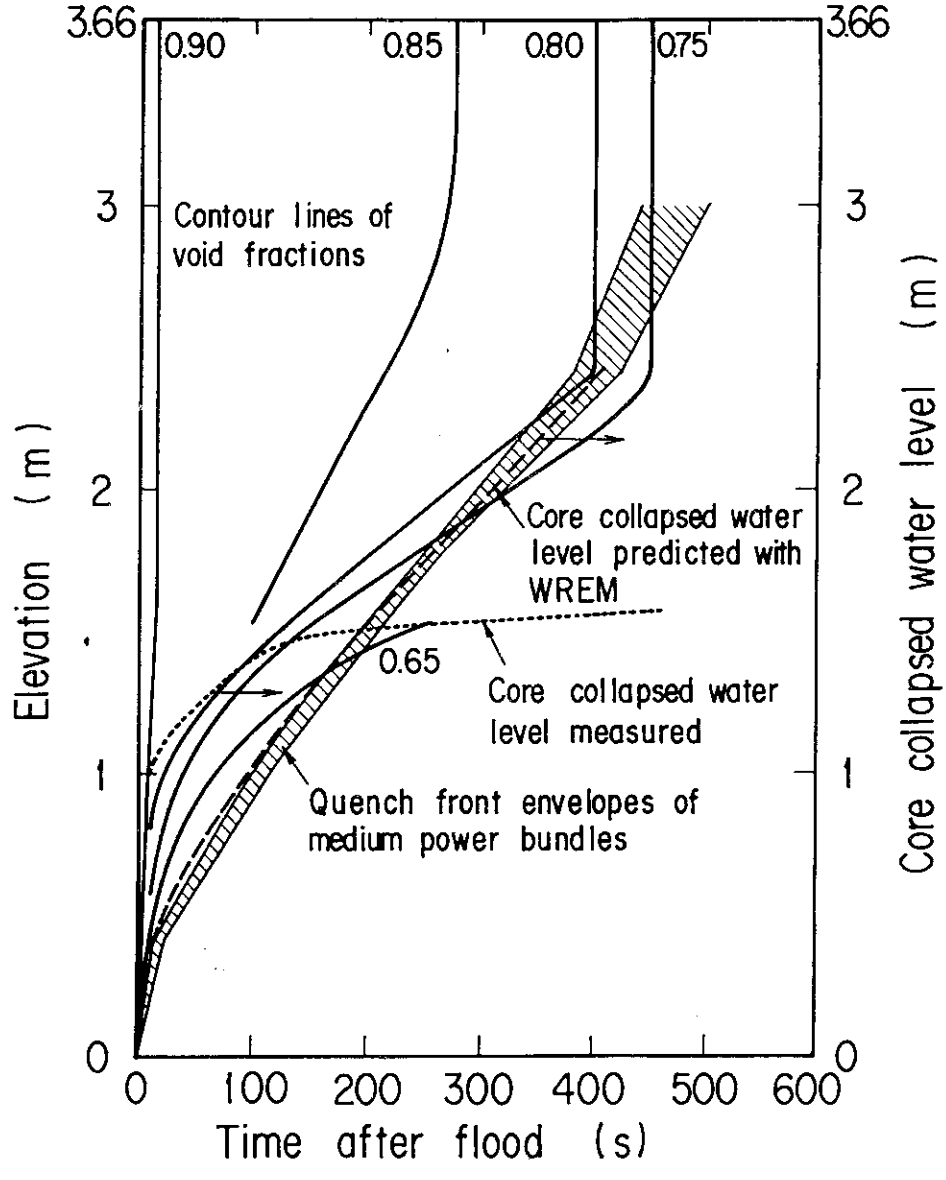


Fig.13 Core collapsed water level, quench front envelopes and contour lines of void fractions

# Appendix A

Explanation of measuring location of referred data and definition of the evaluated data

Figure list

1. Definition of Tag.ID for clad surface temperatures

Notation : TENNWAM

NN : Bundle number

WA : Power zone

WA = X1, X2 : High power (Local power factor 1.1)

WA = Y1, Y2 : Medium power (Local power factor 1.0)

WA = Z1, Z2 : Low power (Local power factor 0.95)

M : Elevation

| | Elevation (m) | Axial power factor |
|---|---|---|
| 1 | 0.38 | 0.568 |
| 2 | 1.015 | 1.176 |
| 3 | 1.83 | 1.492 |
| 4 | 2.44 | 1.312 |
| 5 | 3.05 | 0.815 |

2. Definition of power zone and bundle number

See Fig. A-1

3. Definition of Tag.ID for void fraction

See Fig. A-2

4. Definition of Tag.ID for average linear power of heater rod in each power unit zone

See Fig. A-3

5. Definition of carry-over rate fraction (CRF)

$$CRF = \frac{\dot{m}_{UP} + \dot{m}_{L}}{\dot{m}_{CR} + \dot{m}_{UP} + \dot{m}_{L}}$$

The calculated data within ±25 s are averaged:

$$(CRF)_i = \frac{1}{101} \sum_{k=i-50}^{i+50} (CRF)_k$$

where

$\Delta P_{UP}$ : Average of measured data at four orientations

$\Delta P_{CR}$ : Same as above

$$\dot{m}_{UP} = A_{up} \frac{d}{dt} (\Delta P_{UP})$$

$$\dot{m}_{CR} = A_{CR} \frac{d}{dt} (\Delta P_{CR})$$

$$\dot{m}_L = \sum_{k=1}^{4} \dot{m}_{pk}$$

$\dot{m}$ : mass flow rate or mass accumulation rate

$\Delta P$: differential pressure

suffix

UP: upper plenum

CR: core

L : loop

p : primary pump

6. Definition of Tag.ID for differential pressure through downcomer, upper plenum, core and lower plenum

See Fig. A-4

7. Definition of Tag.ID for differential pressure through intact and broken loop and broken cold leg nozzle

See Fig. A-5

8. Definition of Tag.ID for fluid temperature in inlet and outlet plenum and secondary of steam generator

See Fig. A-6

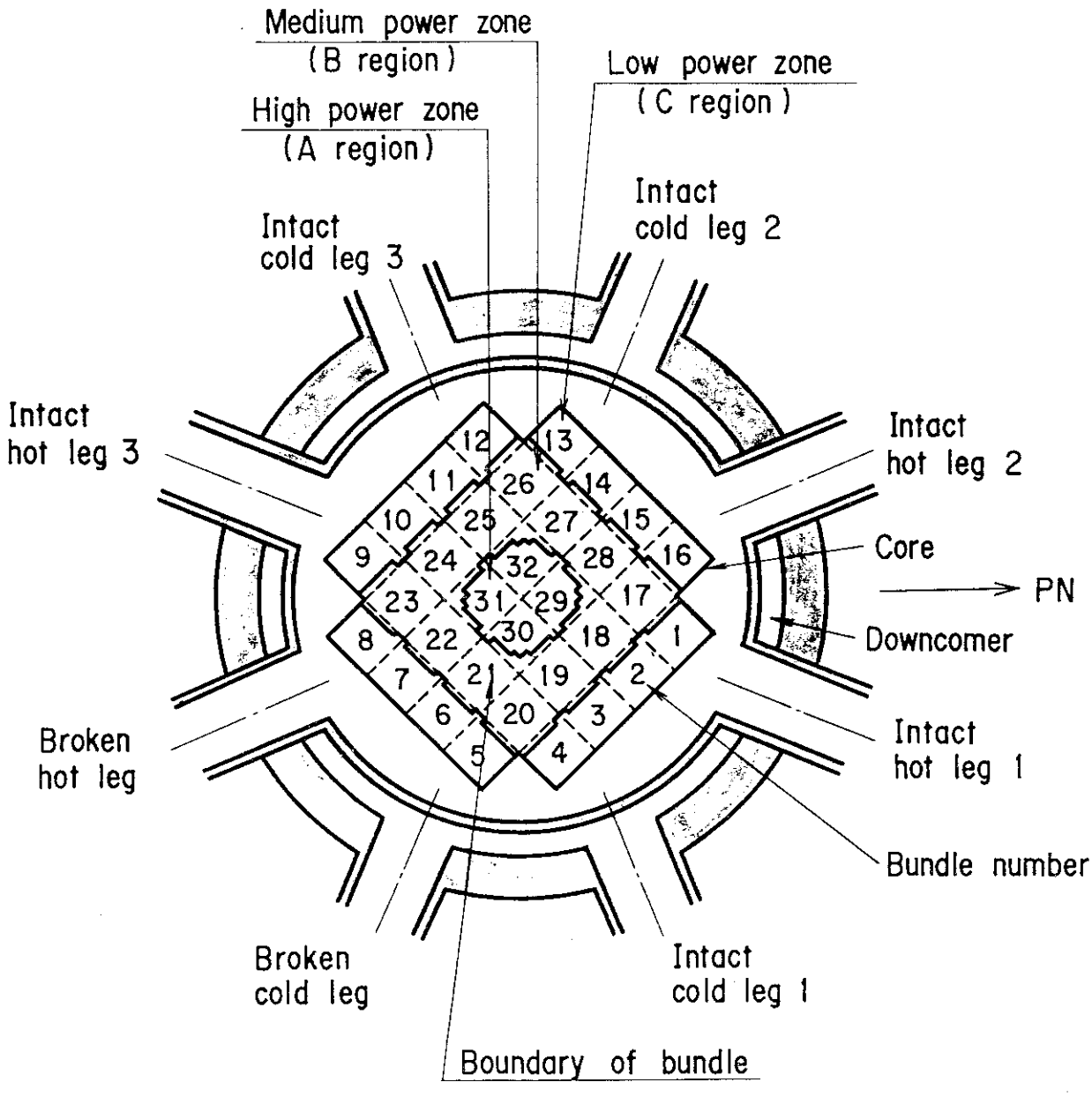


Fig.A－1 Definition of power zones and bundle numbers

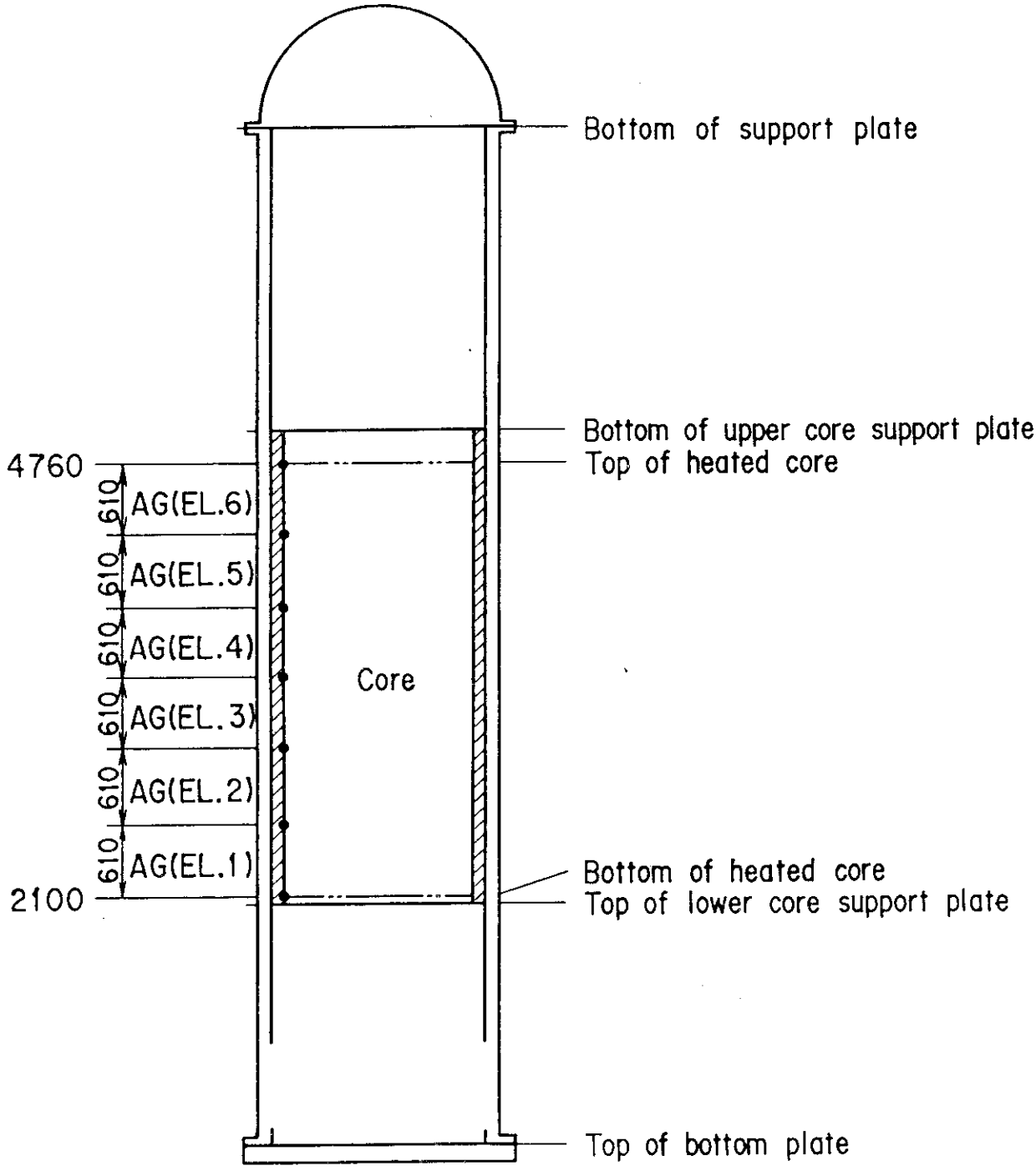


Fig. A－2 Definition of Tag. ID for void fraction (AG(EL.1)～AG(EL.6))

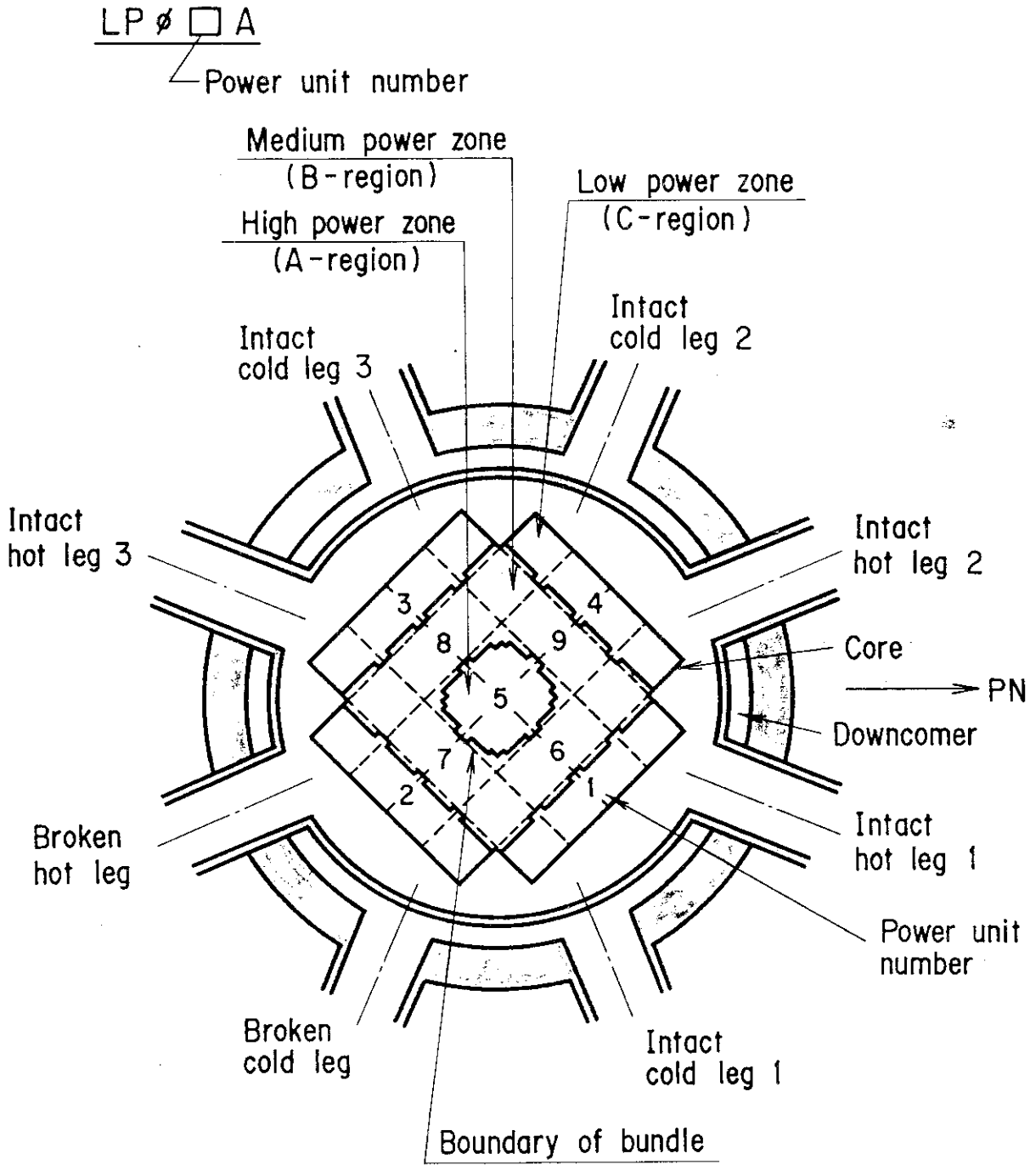


Fig. A－3 Definition of Tag. ID for average linear power of heater rod in each power unit zone (LP01A～LP09A)

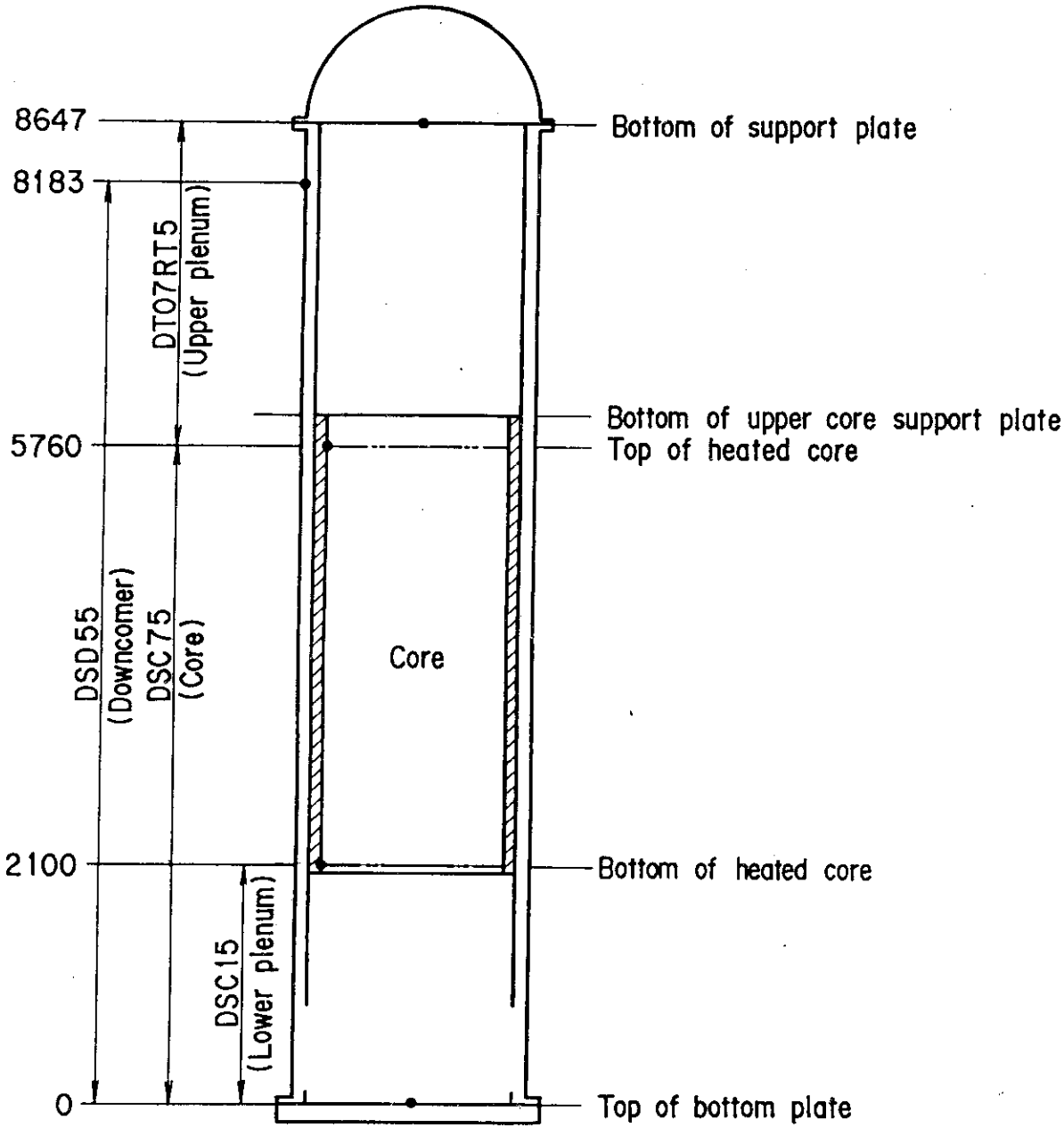


Fig. A－4 Definition of Tag. ID for differential pressure through downcomer, upper plenum, core, and lower plenum
(DSD 55, DTO7RT5, DSC75, DSC15)

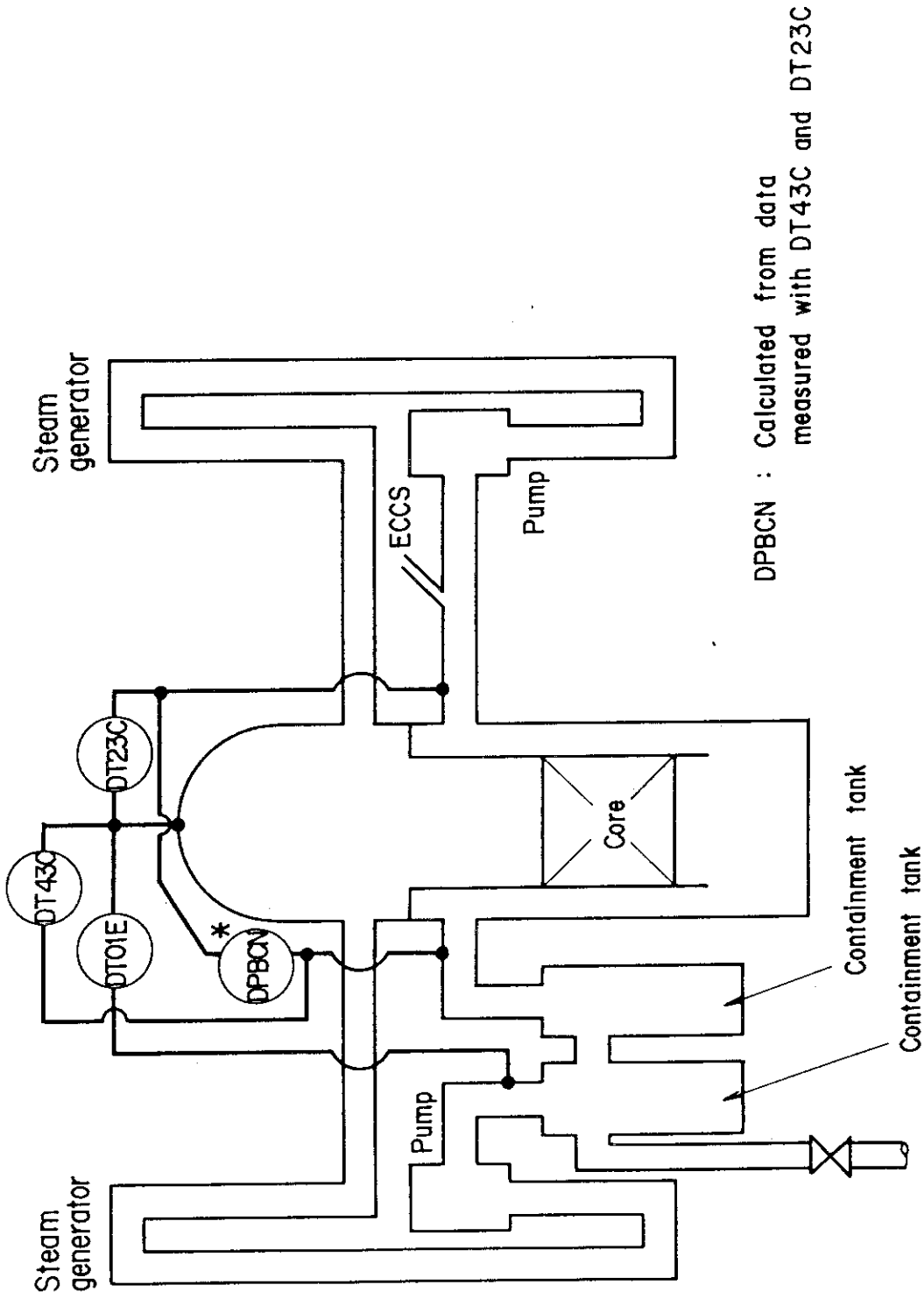


Fig. A－5 Definition of Tag. ID for differential pressure through intact and broken loop and broken cold leg nozzle (DT23C, DT01B, DPBCN)

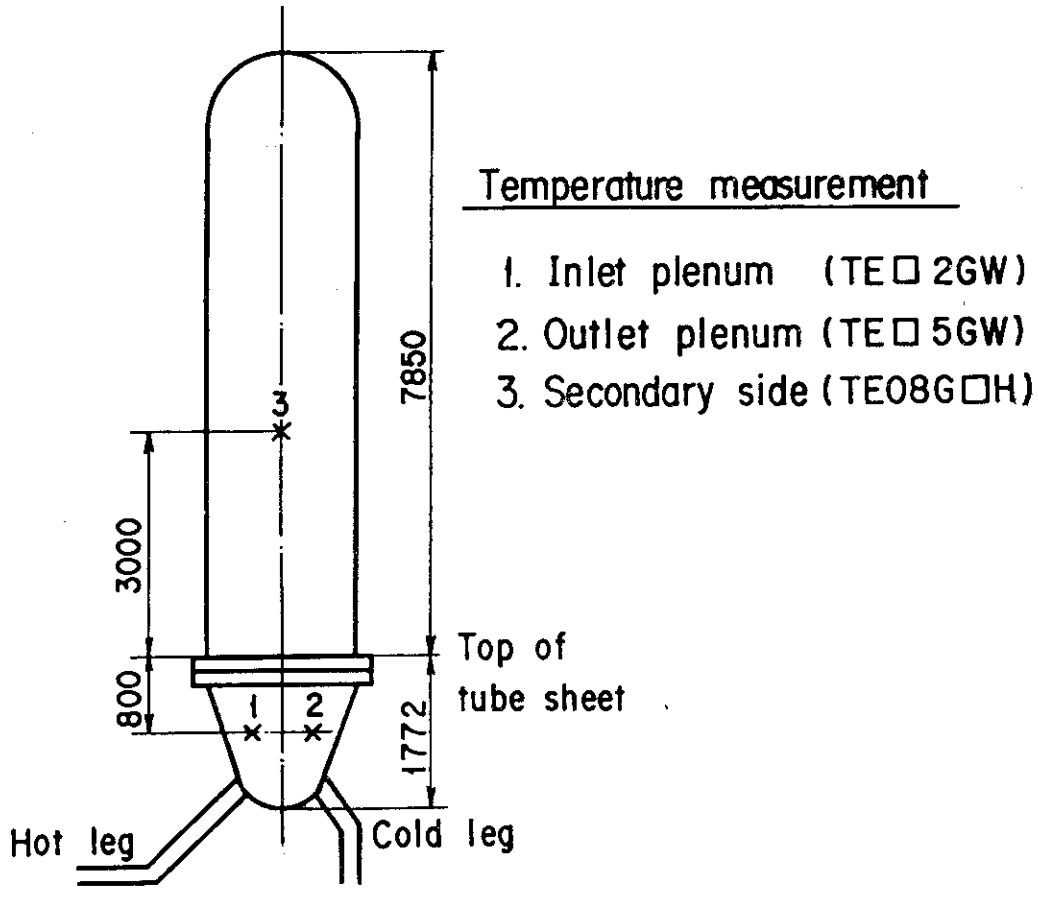


Fig. A－6 Definition of Tag. ID for fluid temperature in inlet and outlet plenum and secondary of steam generator (TE□2GW, TE□5GW, TE08G□H)

# Appendix B

## Main results of test C1-19 (Run 38)

Table and Figure List

Table B-1 Summary of test conditions

1. TEST TYPE : EVALUATION MODEL TEST
2. TEST NUMBER : RUN 038 3. DATE : March 18, 1981
4. POWER : A: TOTAL: 9.28 MW; B:LINEAR: 1.39 KW/M
5. RELATIVE RADIAL POWER SHAPE :

   A: ZONE: A B C

   B: RATIO: 1.299 1.092 0.841
6. AXIAL POWER SHAPE : CHOPPED COSINE
7. PRESSURE ($KG/CM^2A$) :

   A: SYSTEM: 2.03, B: CONTAINMENT 2.03,

   C: STEAM GENERATOR SECONDARY: 53.2
8. TEMPERATURE (DEG.C) :

   A: DOWNCOMER WALL 169, B: VESSEL INTERNALS 115,

   C: PRIMARY PIPING WALL 123, D: LOWER PELNUM LIQUID 114,

   E: ECC LIQUID 38.1, F: STEAM GENERATOR SECONDARY 263,

   G: CORE TEMPERATURE AT ECC INITIATION 844
9. ECC INJECTION TYPE: C

   A: COLD LEG, B: LOWER PLENUM, C: LOWER PLENUM + COLD LEG
10. PUMP K-FACTOR : ∿ 15
11. ECC FLOW RATES AND DURATION :

    A: ACCUMULATOR 372 $M^3/HR$ FROM 0 TO 25.5 SECONDS

    B: LPCI 40.5 $M^3/HR$ FROM 25.5 TO 737 SECONDS

    C: ECC INJECTION TO LOWER PLENUM : FROM 0 TO 14 SECONDS

    (VALVE OPENING AND CLOSING TIMES ARE INCLUDED IN THE INJECTION DURATION)
12. INITIAL WATER LEVEL IN LOWER PLENUM : 0.89 M.
13. POWER CONTROL : ANS x 1.2 + ACTINIDE ( 30 SEC AFTER SCRAM)
14. EXPECTED BOCREC TIME FROM ECC INITIATION 9 SEC
15. EXPECTED PEAK TEMPERATURE AT BOCREC 870 C

Table B-2 Chronology of events

| EVENT | TIME (sec) |
|---|---|
| Test Initiated (Heater Rods Power on) (Data Recording Initiated) | 0 |
| Accumulator Injection Initiated | 93 |
| Power Decay Initiated (Bottom of Core Recovery) | 102 (102) |
| Accumulator Injection Switched from Lower Plenum to Cold Leg | 107 |
| Accumulator Injection Ended and LPCI Injection Initiated | 118.5 |
| All Heater Rods Quenched | 615 |
| Power Off | 710 |
| LPCI Injection Ended | 830 |
| Test Ended (Data Recording Ended) | 1047 |

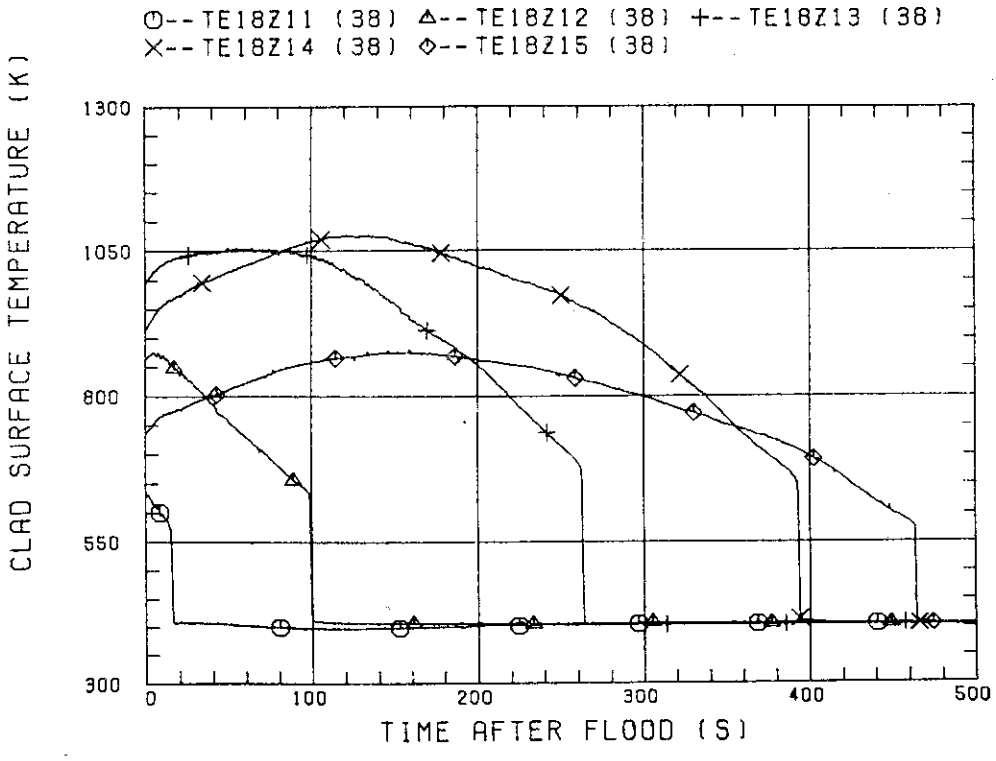


Fig. B-1 Surface temperature on low power rod (Z-rod) in medium power region (B region) (average power rod)

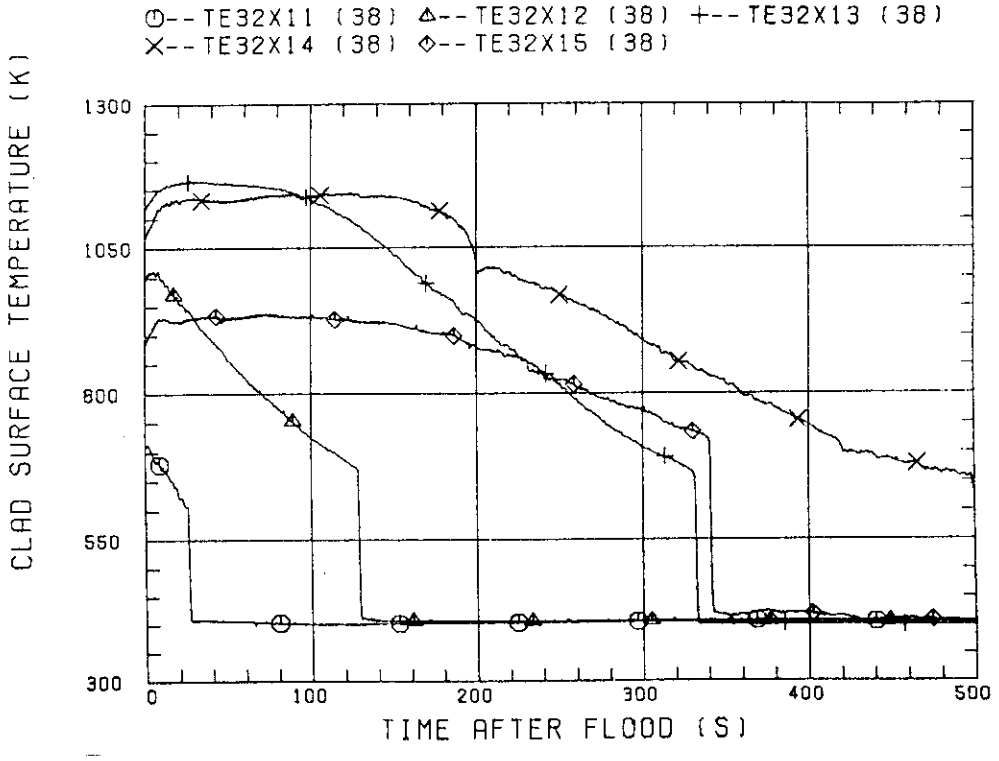


Fig. B-2 Surface temperature on high power rod (X-rod) in high power region (A region) (peak power rod)

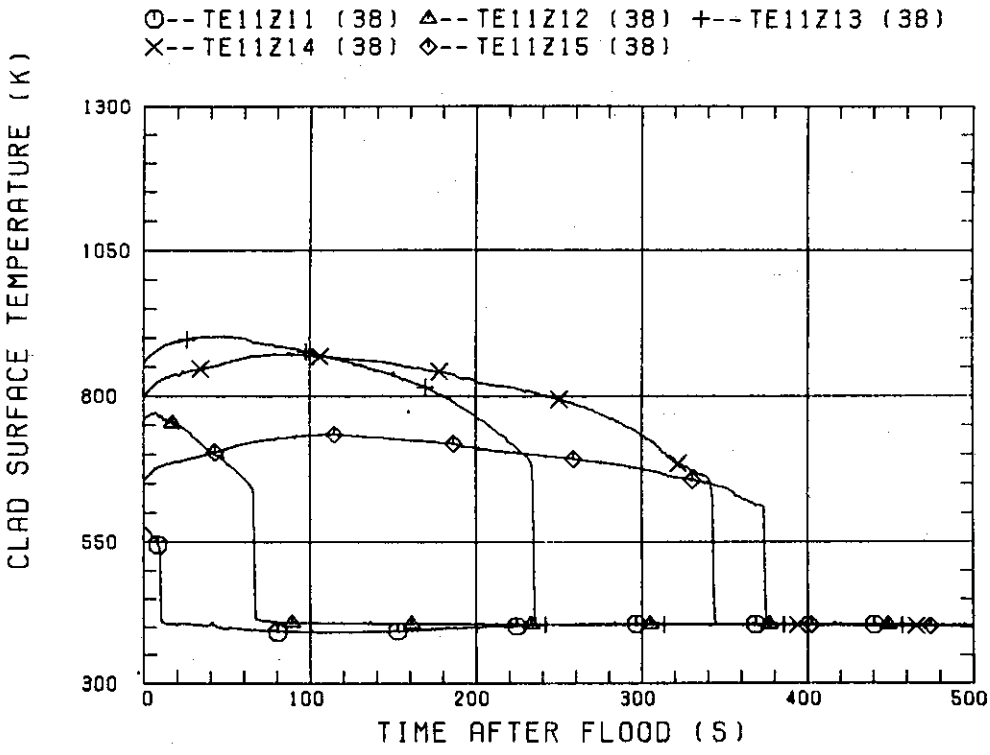


Fig. B-3 Surface temperature on low power rod (Z-rod) in low power region (C region) (lowest power rod)

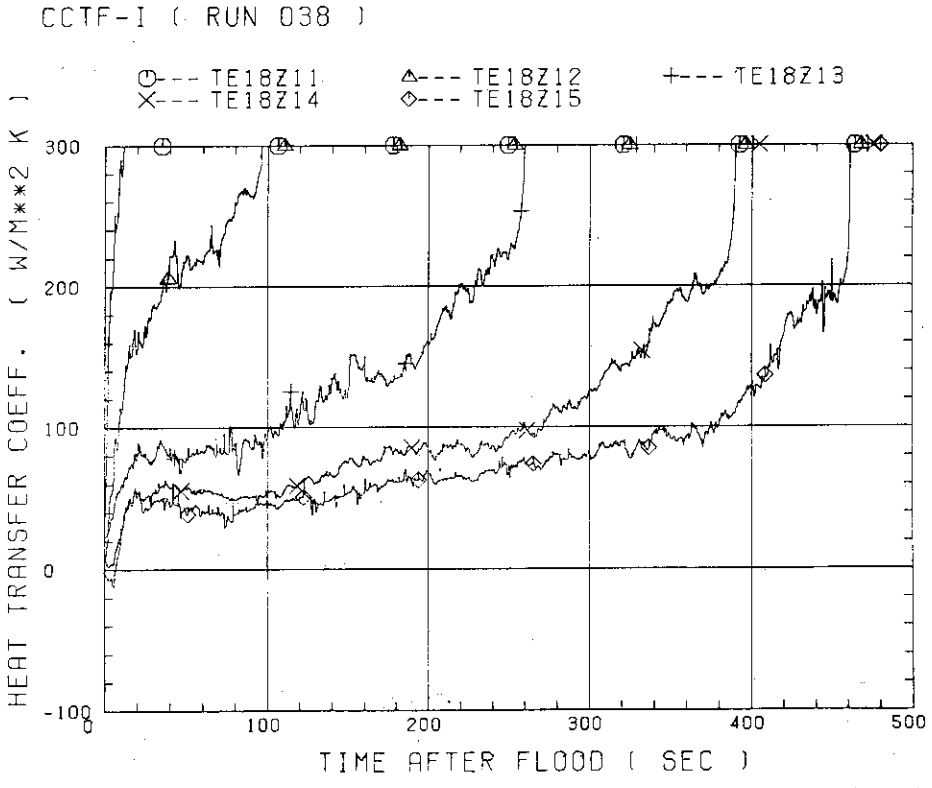


Fig. B-4 Heat transfer coefficient at midplane of low power rod (Z-rod) in medium power region (B region) (average power rod)

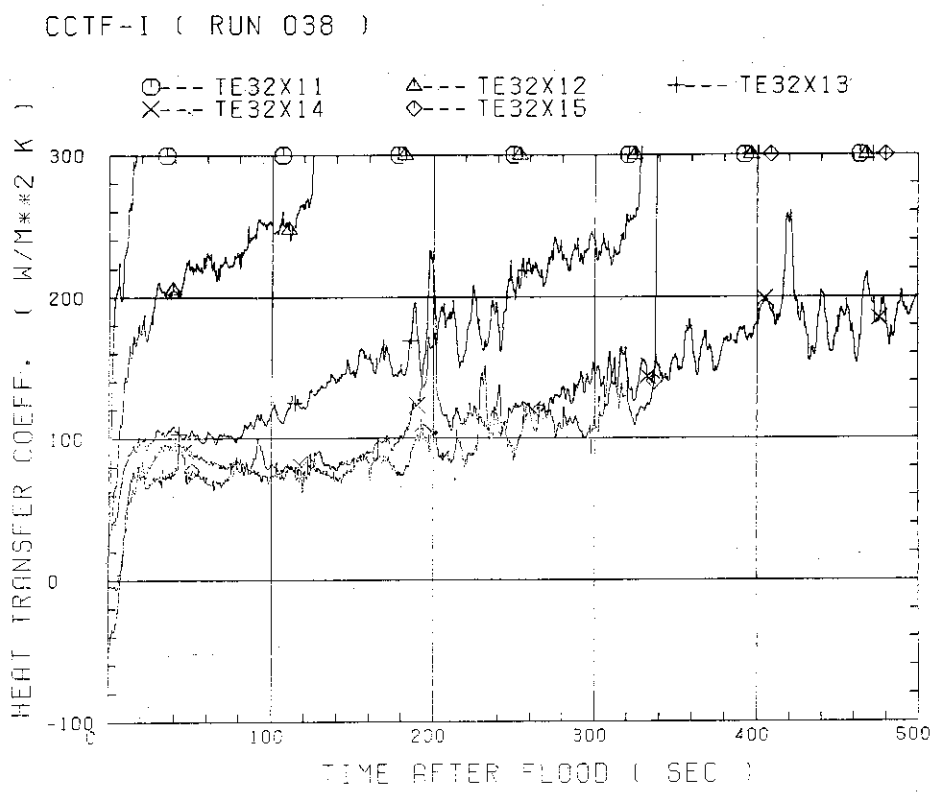


**Fig. B-5** Heat transfer coefficient at midplane of high power rod (X-rod) in high power region (A region) (peak power rod)

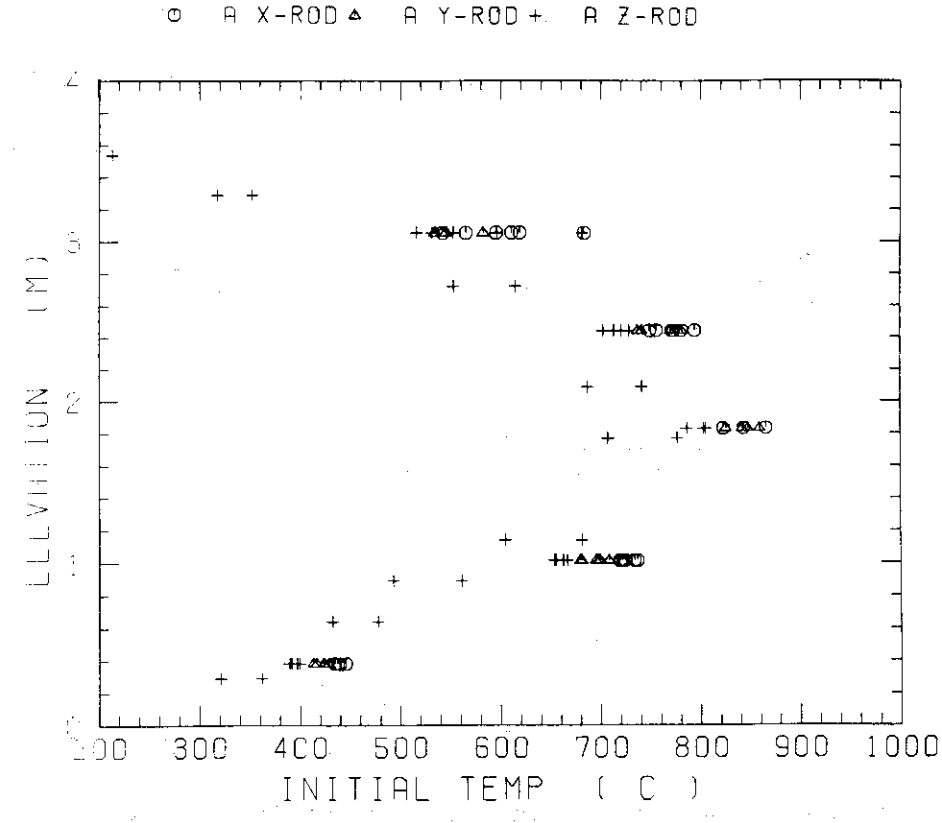


Fig. B-6 Initial rod surface temperature in high power region (A region)

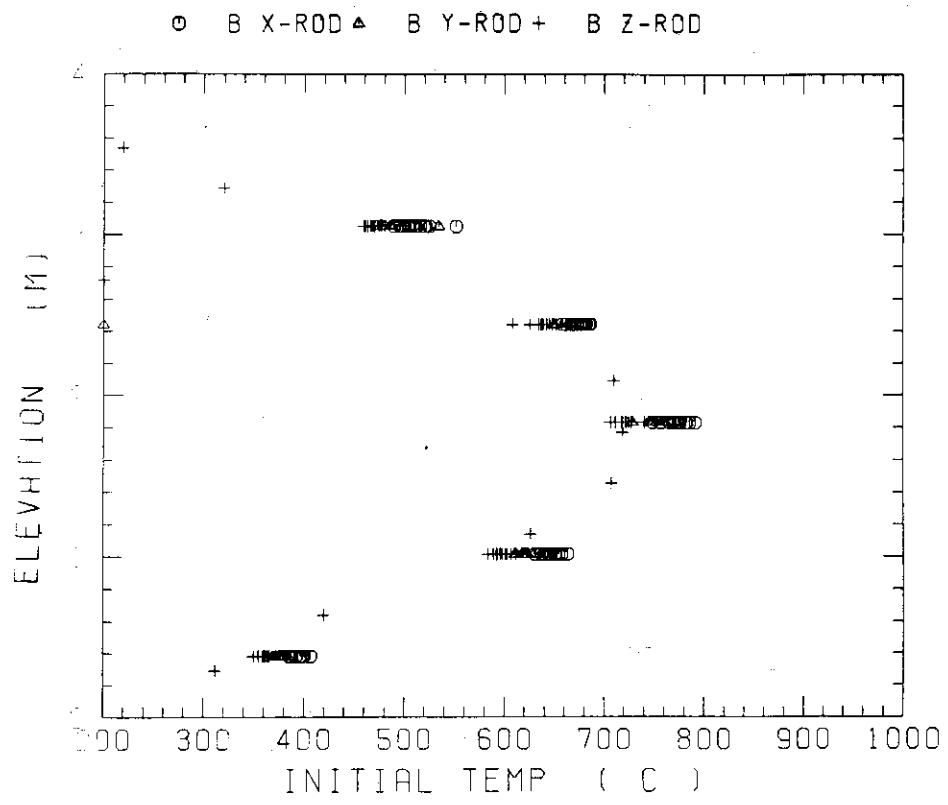


Fig. B-7 Initial rod surface temperature in medium power region (B region)

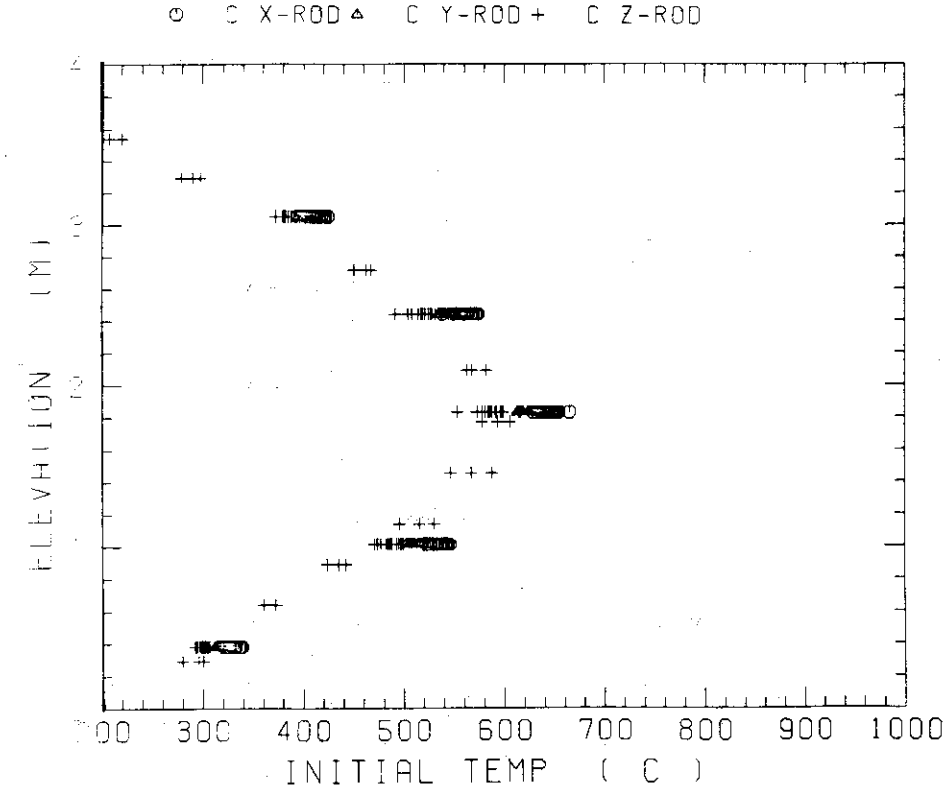


Fig. B-8 Initial rod surface temperature in low power region (C region)

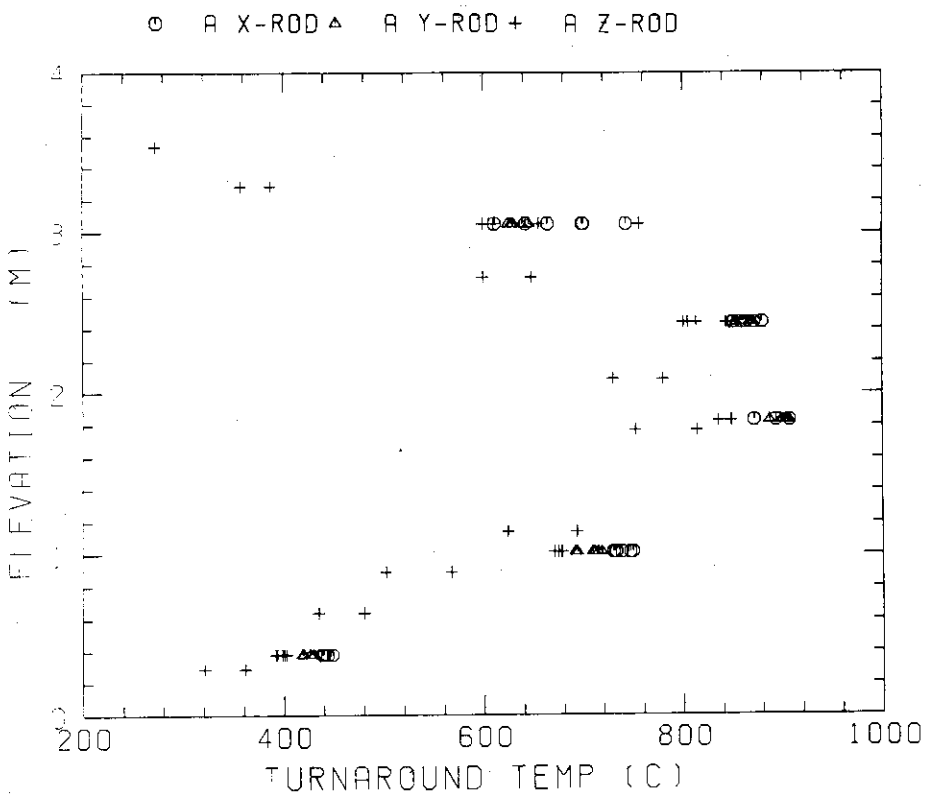


Fig. B-9 Turnaround temperature in high power region (A region)

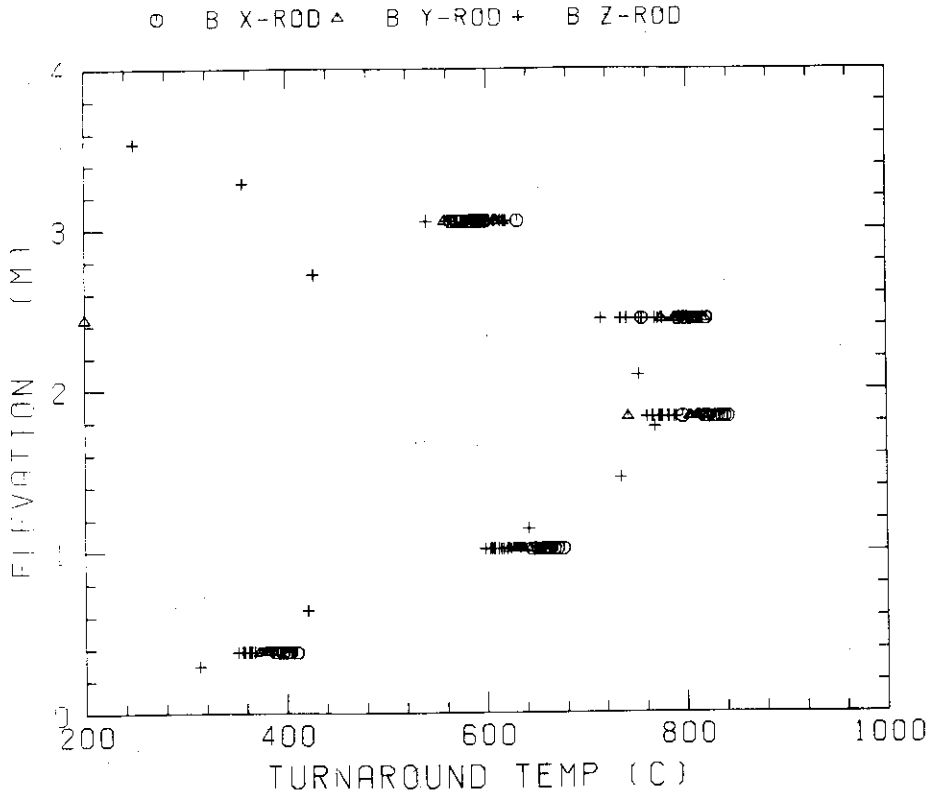


Fig. B-10 Turnaround temperature in medium power region (B region)

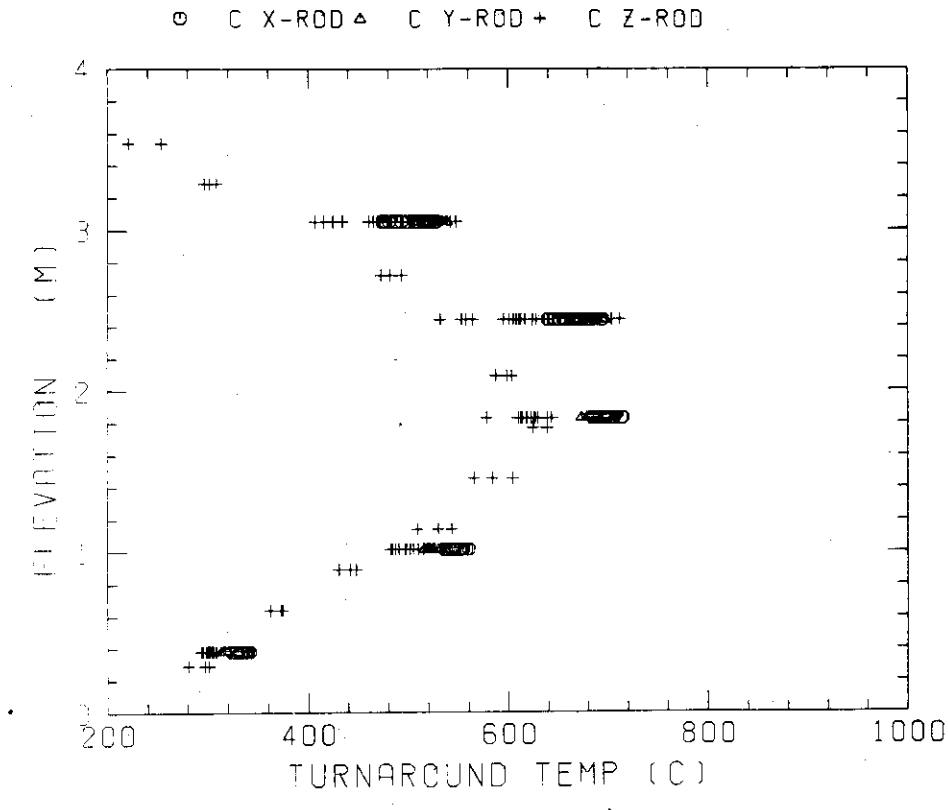


Fig. B-11 Turnaround temperature in low power region (C region)

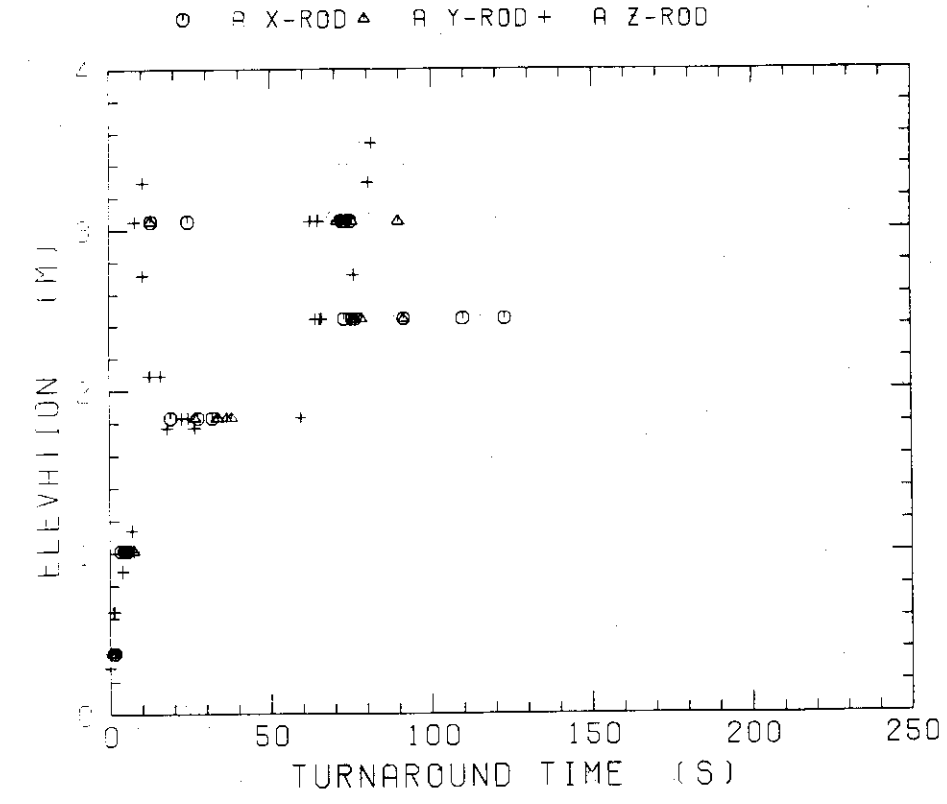


Fig. B-12 Turnaround time in high power region (A region)

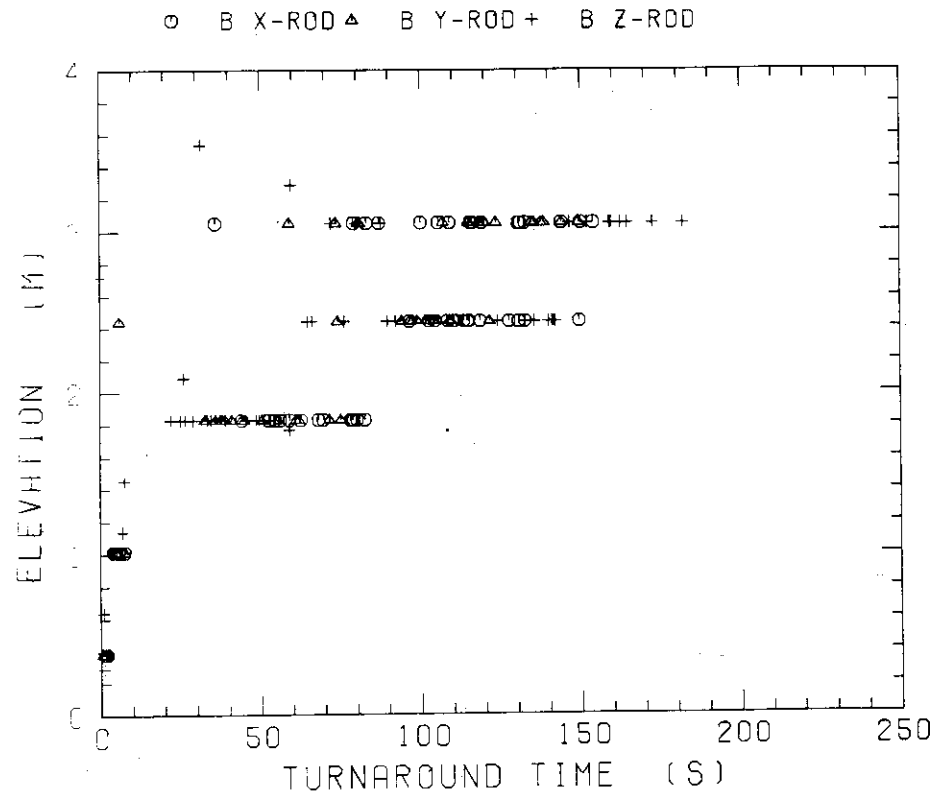


Fig. B-13 Turnaround time in medium power region (B region)

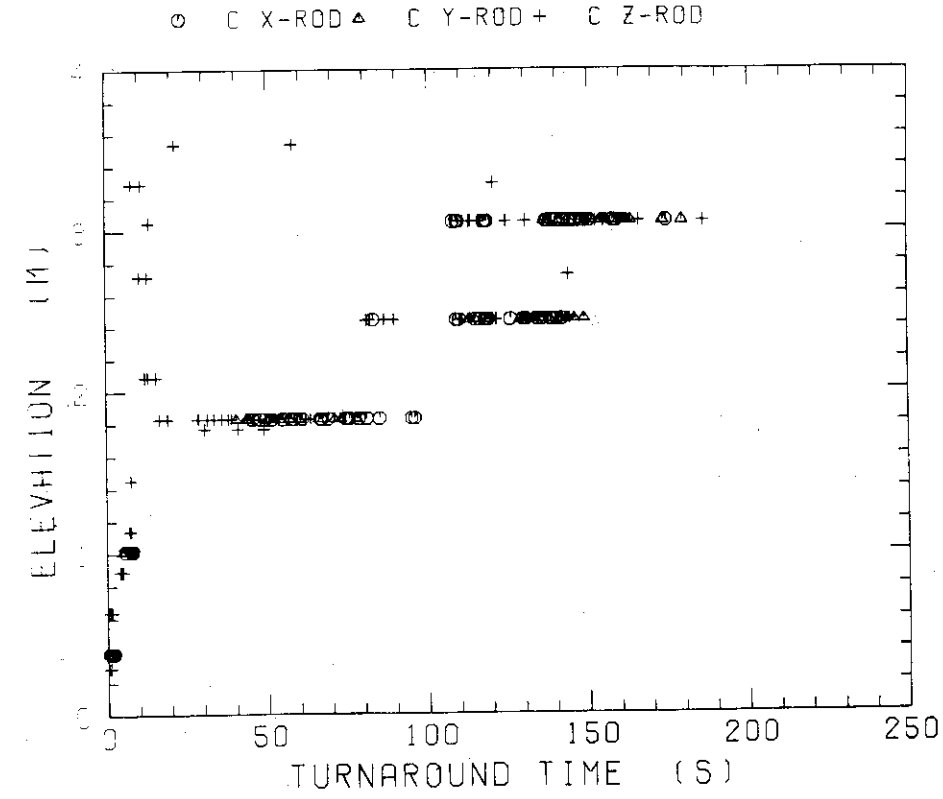


Fig. B-14 Turnaround time in low power region (C region)

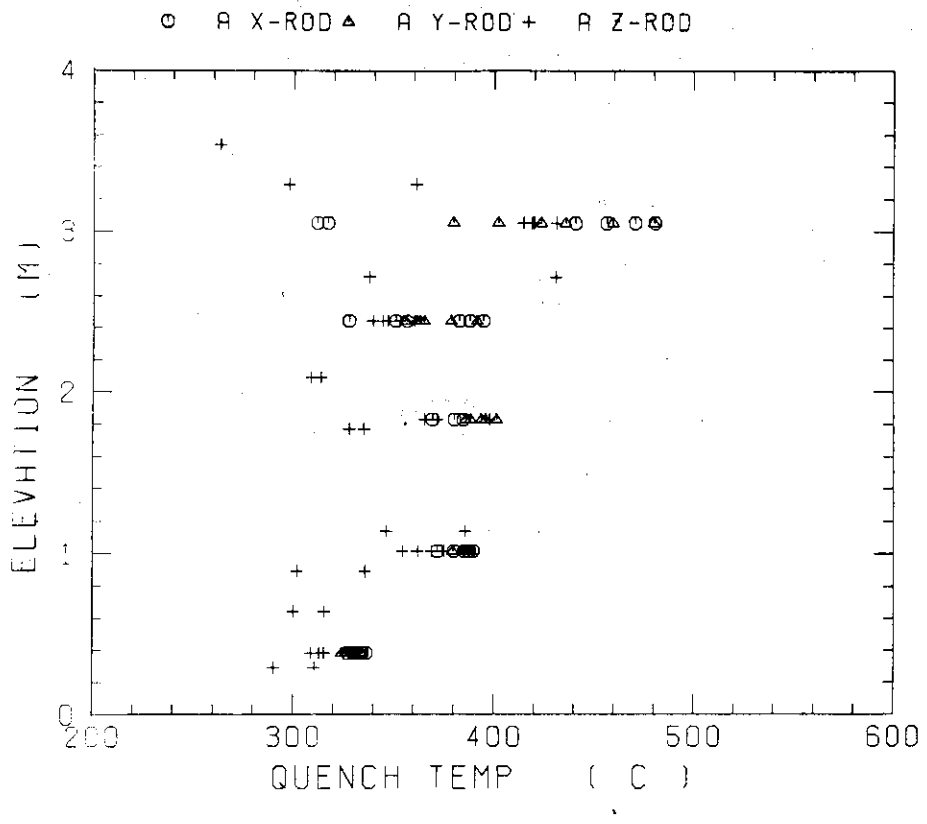


Fig. B-15 Quench temperature in high power region (A region)

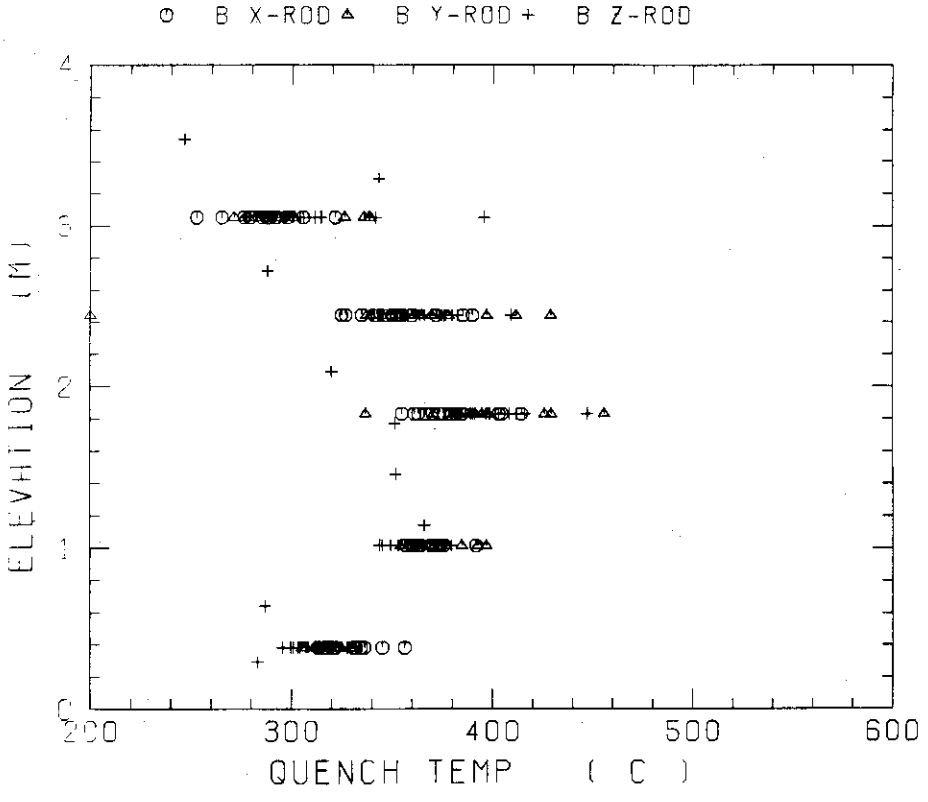


Fig. B-16 Quench temperature in medium power region (B region)

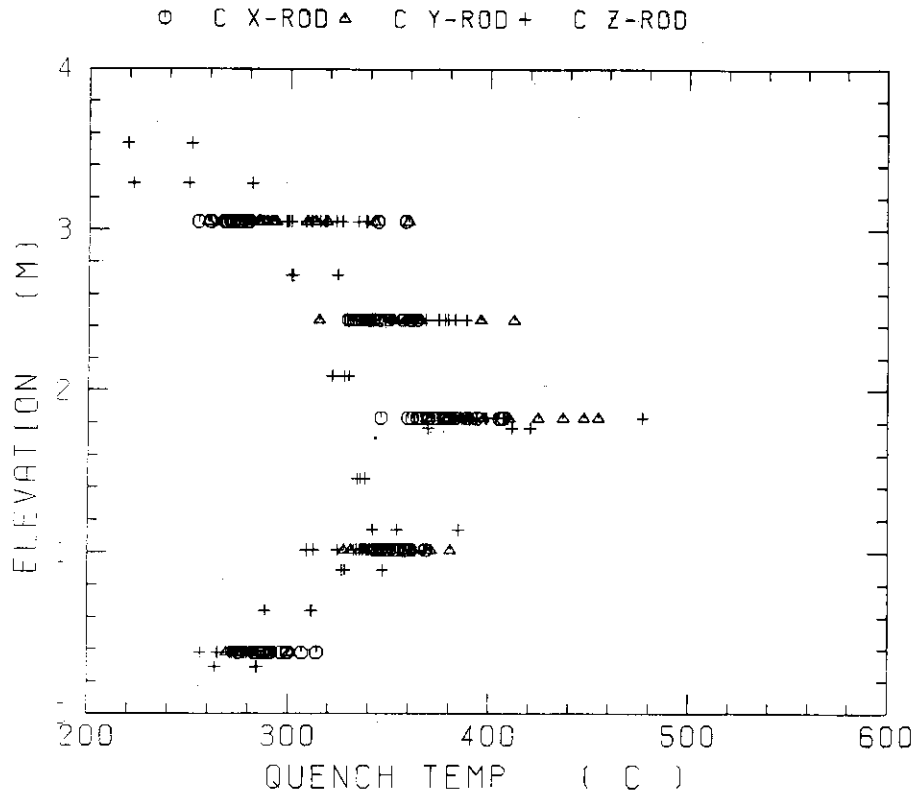


Fig. B-17 Quench temperature in low power region (C region)

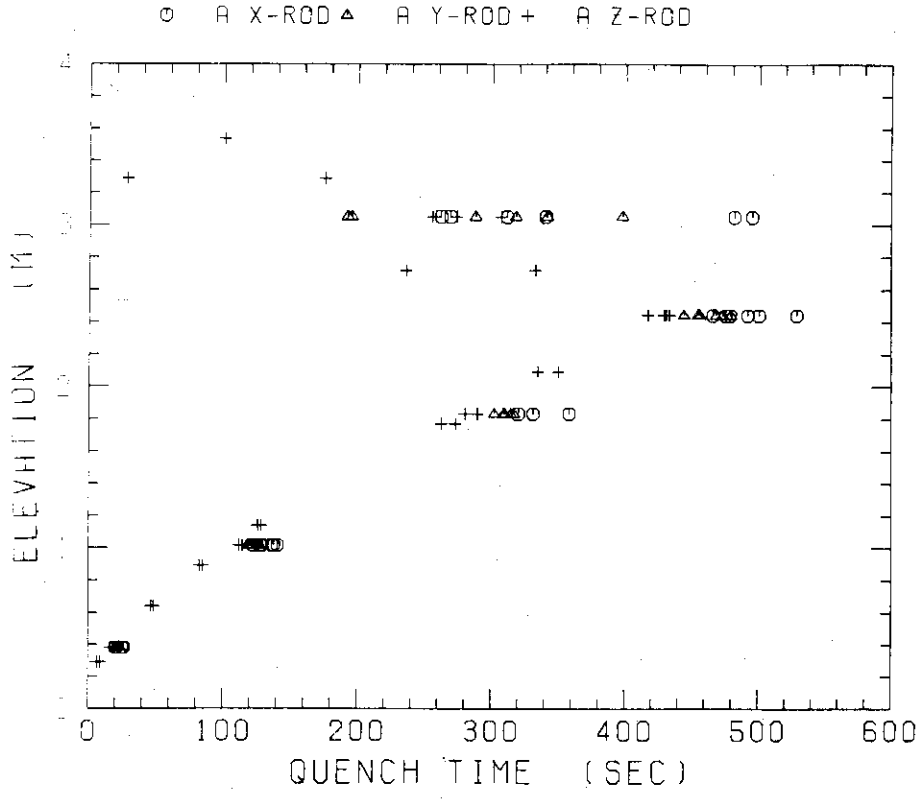


Fig. B-18 Quench time in high power region (A region)

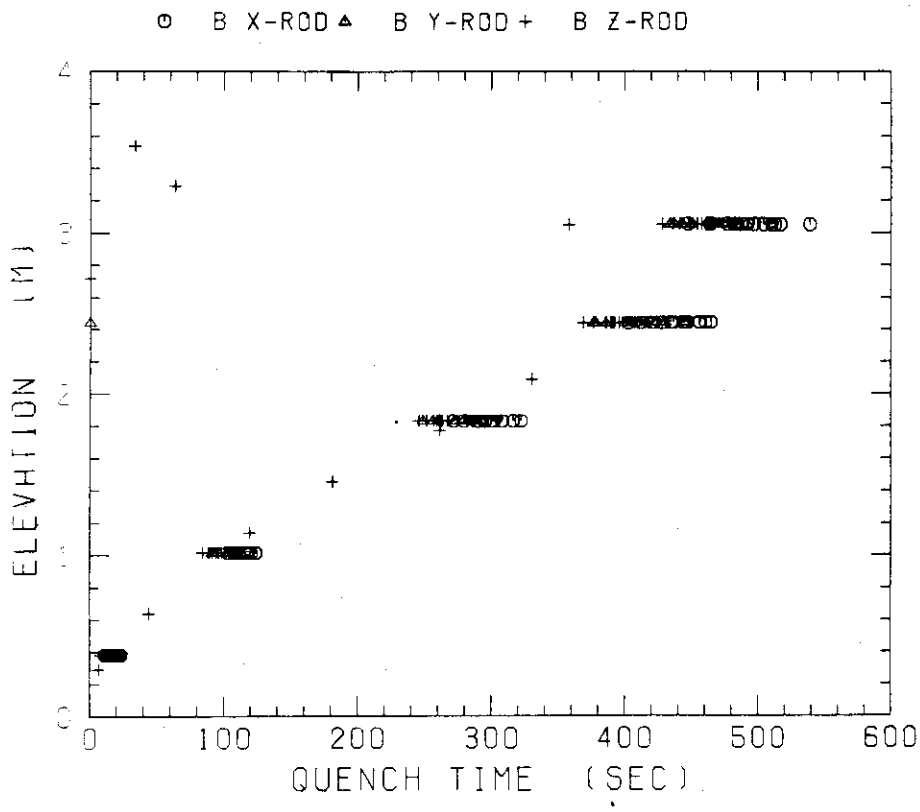


Fig. B-19 Quench time in medium power region (B region)

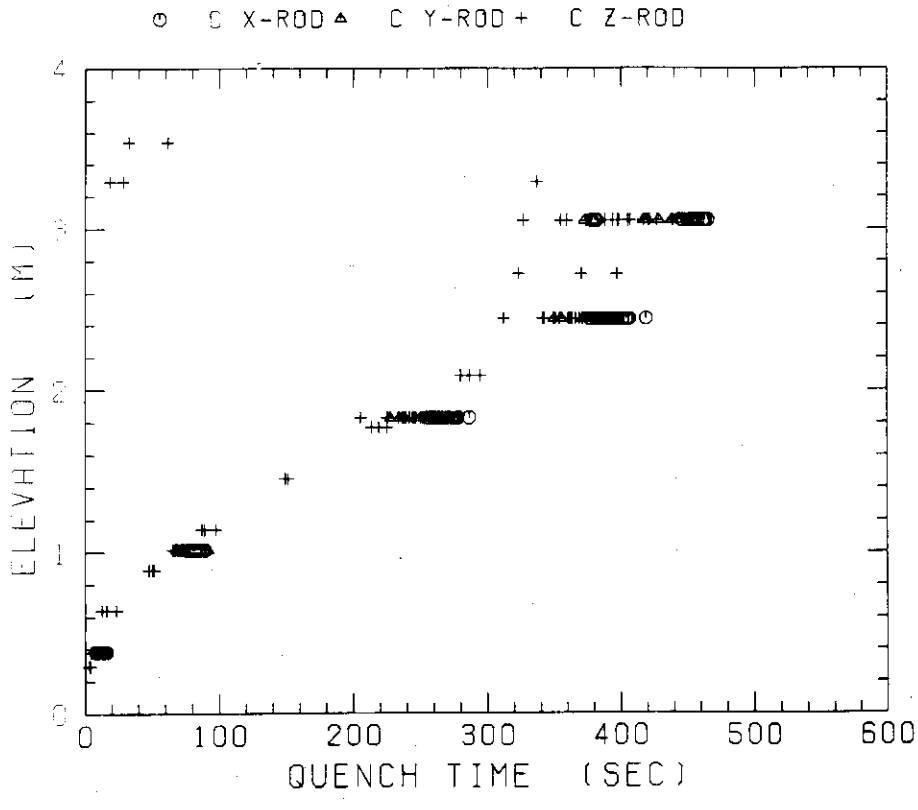


Fig. B-20 Quench time in low power region (C region)

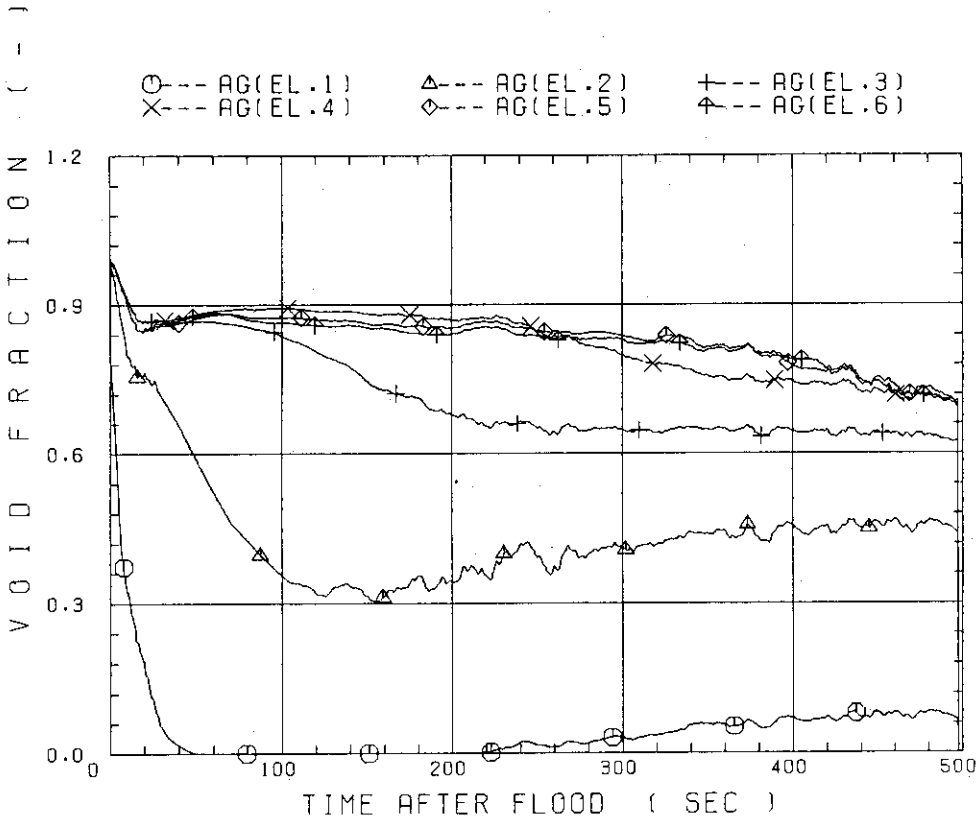


Fig. B-21 Void fraction in core

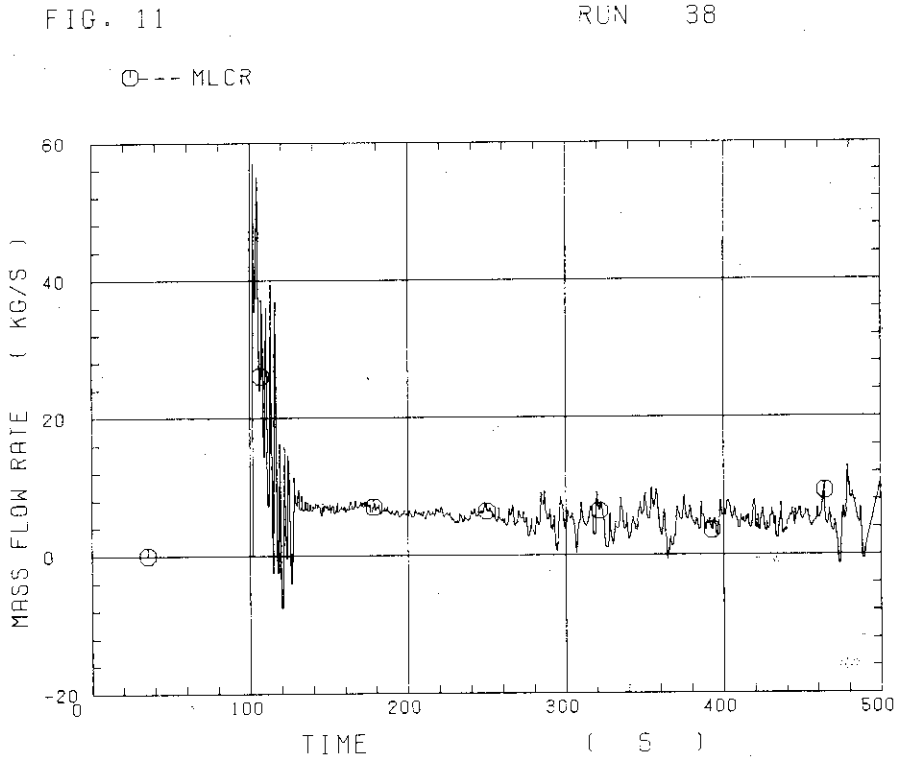


Fig. B-22 Core inlet mass flow rate

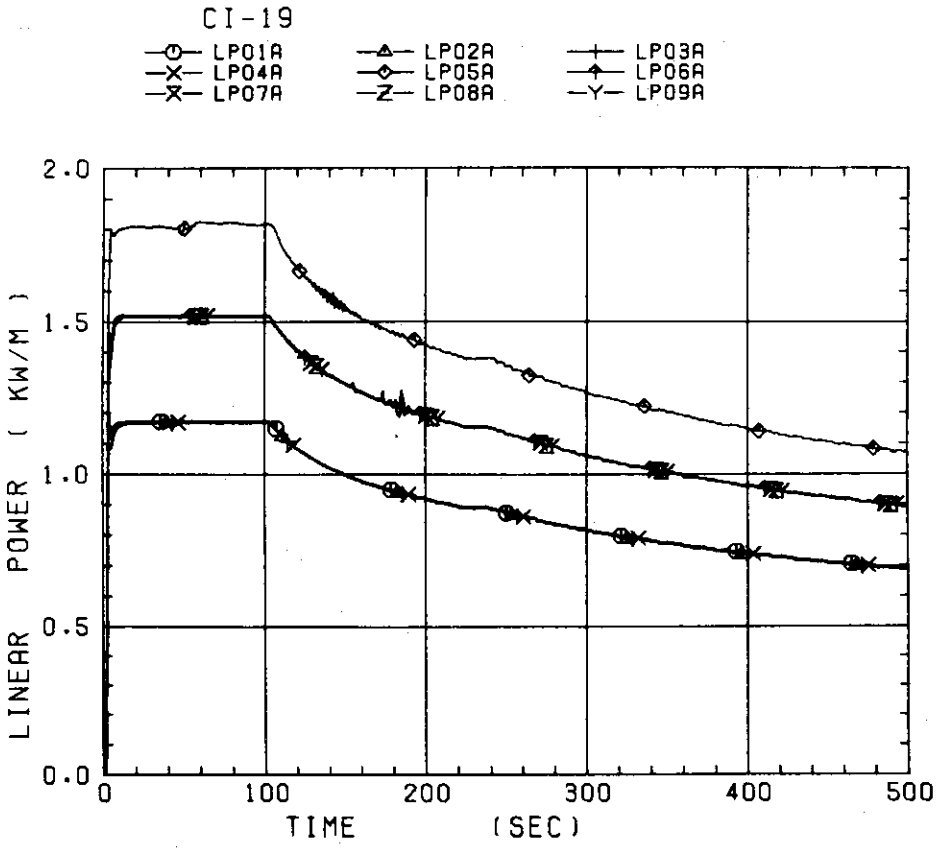


Fig. B-23 Average linear power of heater rod in each power unit zone

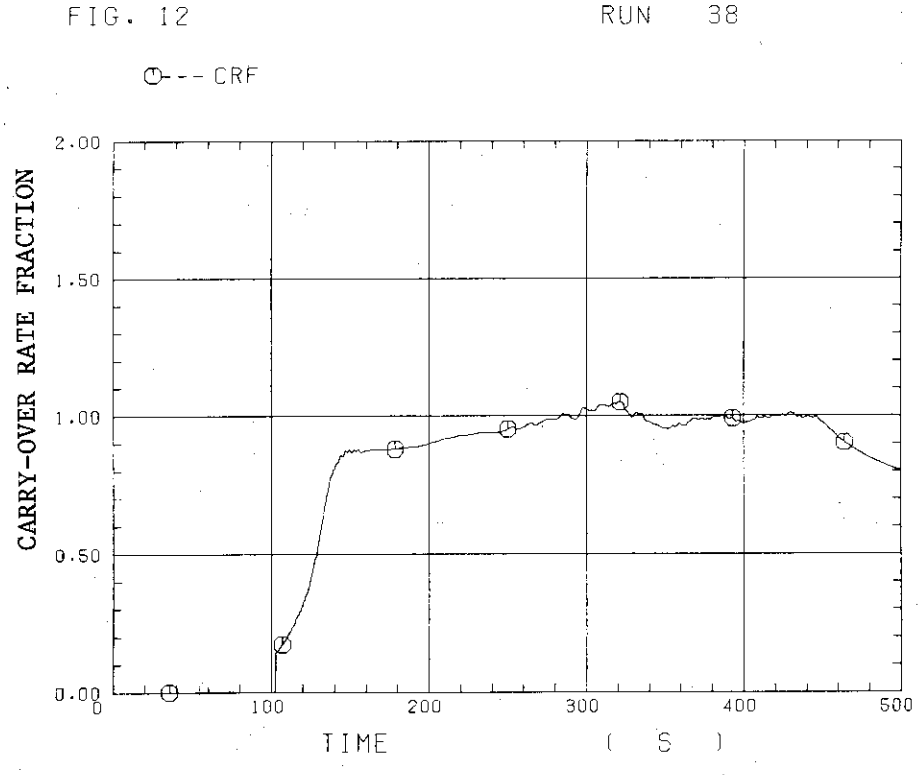


Fig. B-24 Carry-over rate fraction

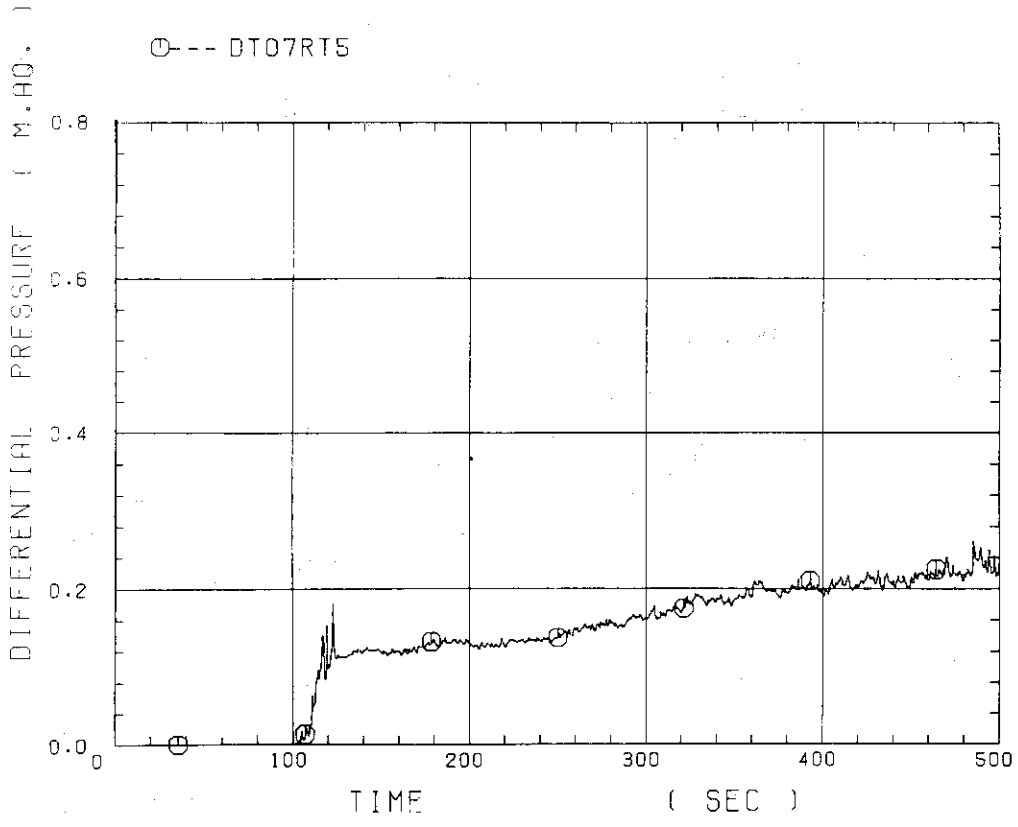


Fig. B-25 Differential pressure through upper plenum

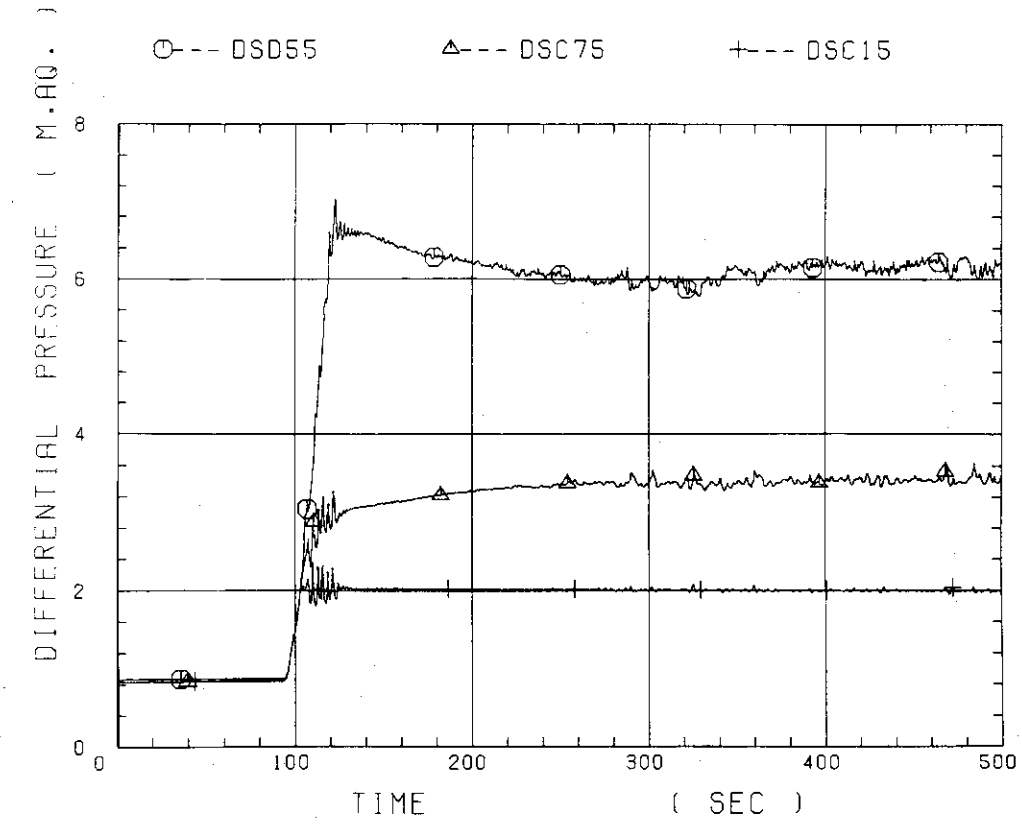


Fig. B-26 Differential pressure through downcomer, core, and lower plenum

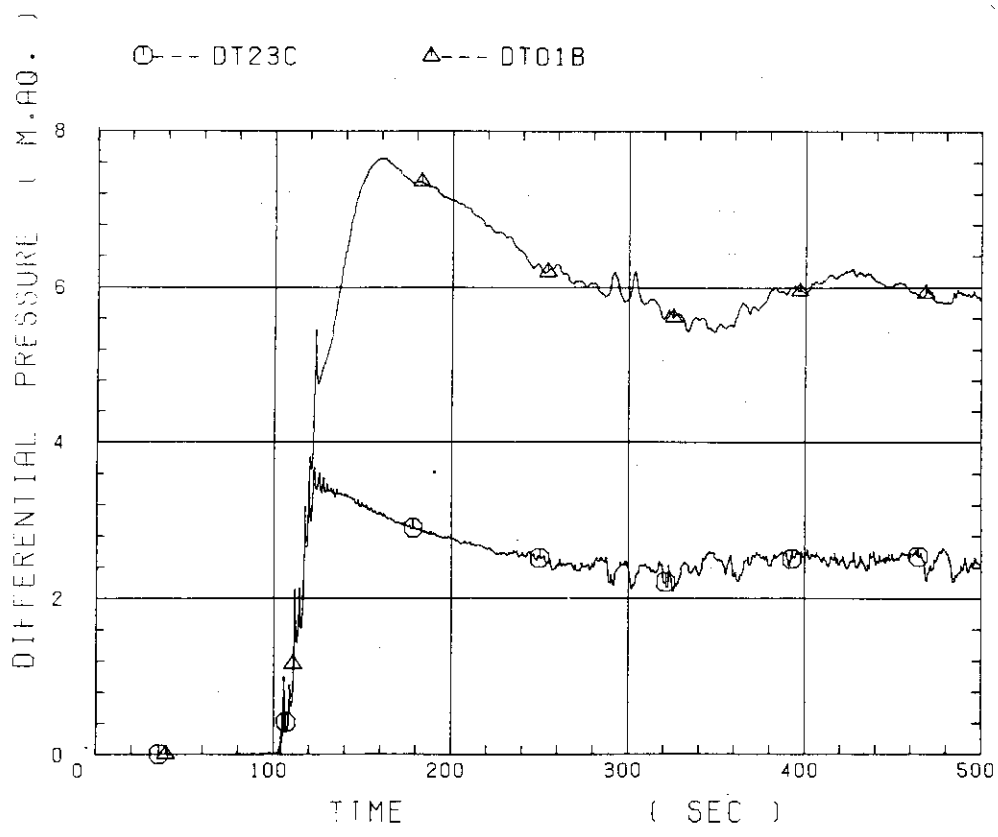


Fig. B-27 Differential pressure through intact and broken loops

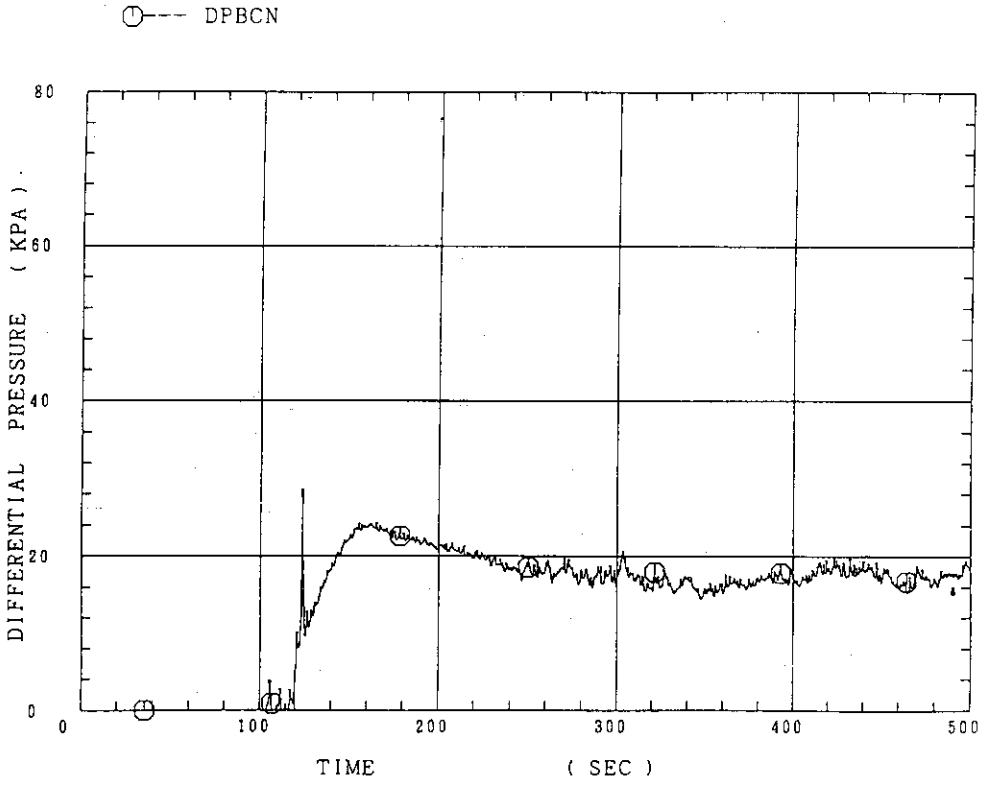


Fig. B-28 Differential pressure through borken cold leg nozzle

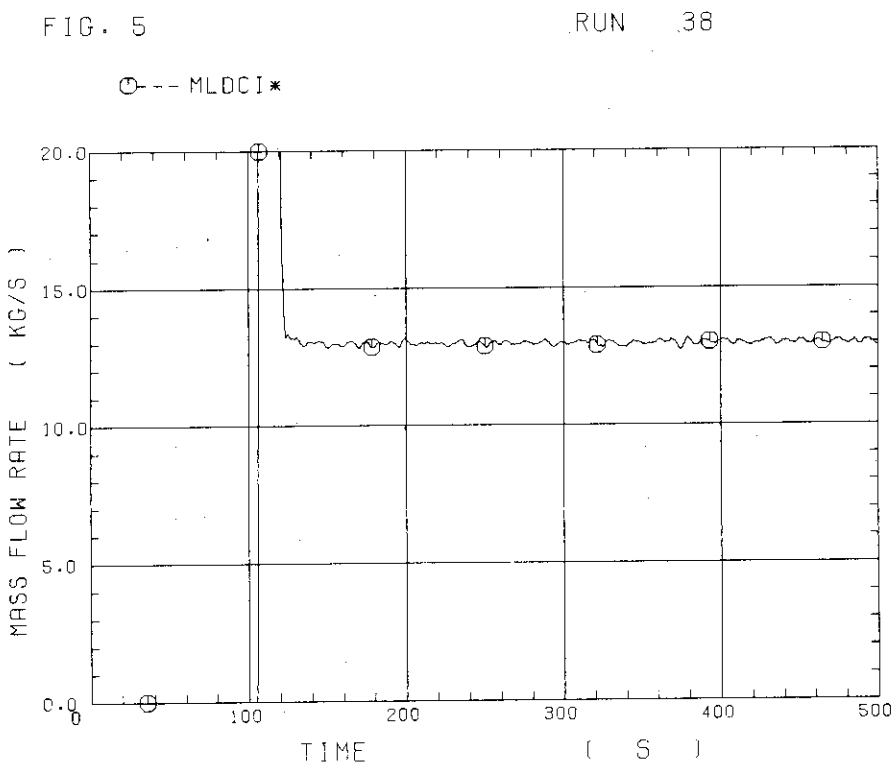


Fig. B-29 Total water mass flow rate from intact loops to downcomer

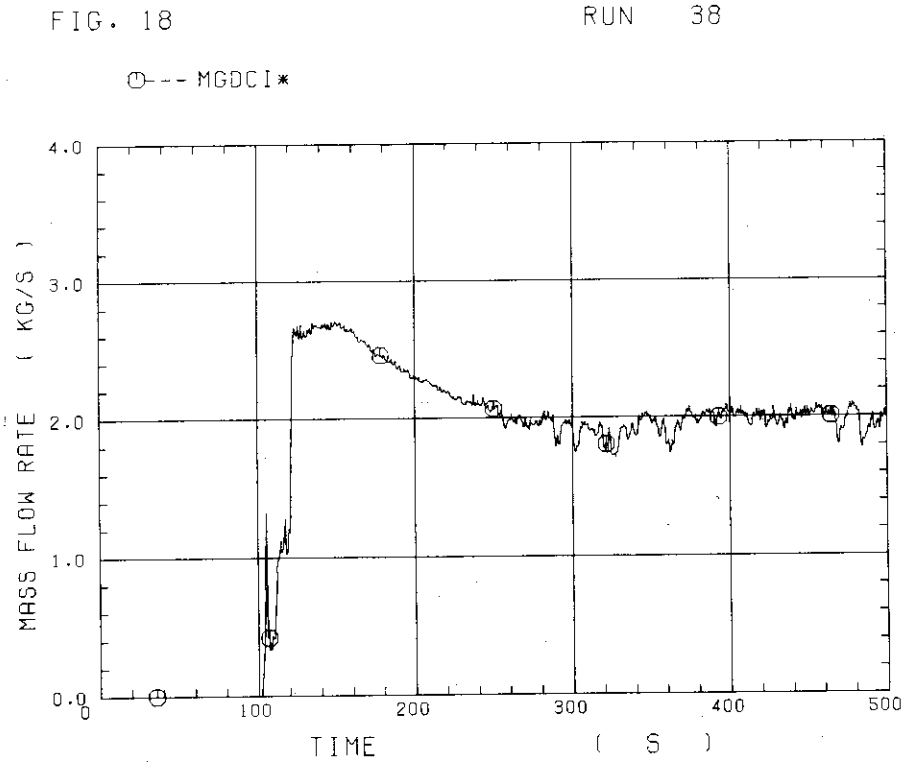


Fig. B-30 Total steam mass flow rate from intact loops to downcomer

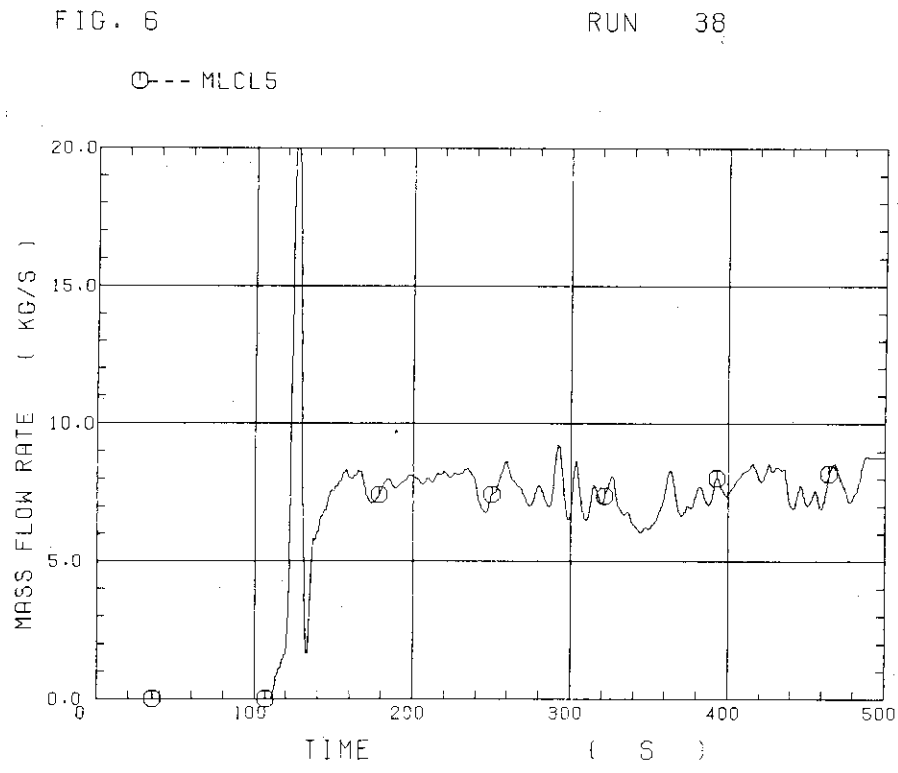


Fig. B-31 Water mass flow rate through broken cold leg nozzle

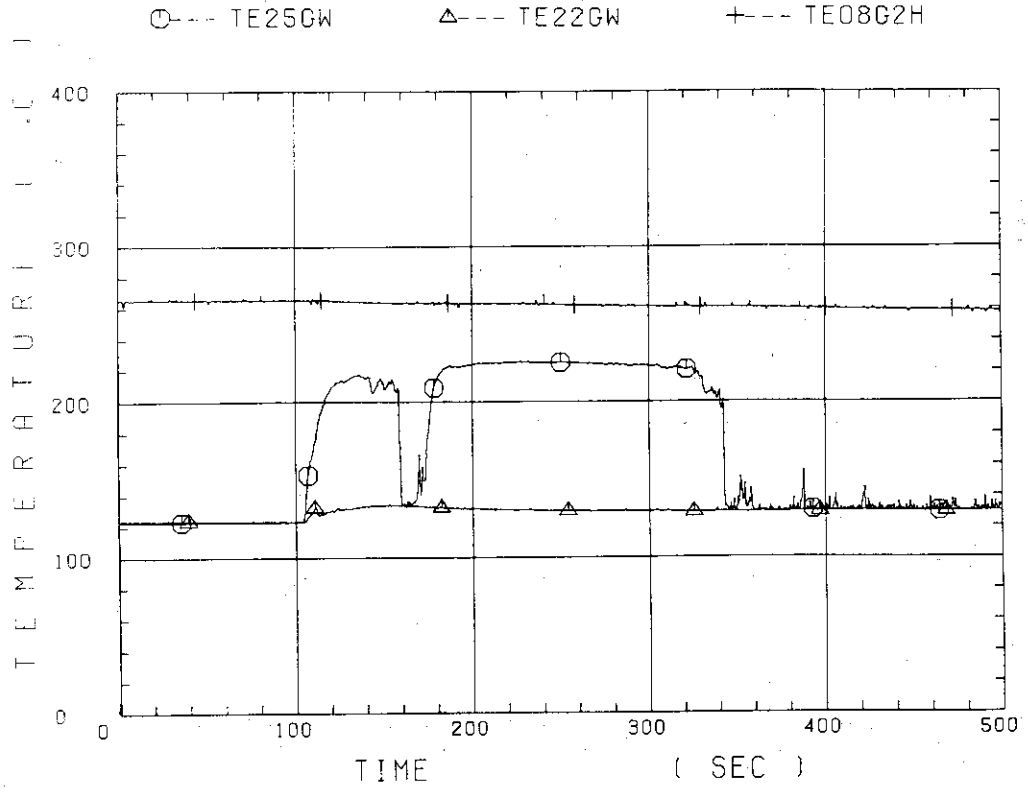


Fig. B-32 Fluid temperature in inlet plenum, outlet plenum, and secondary of steam generator 1

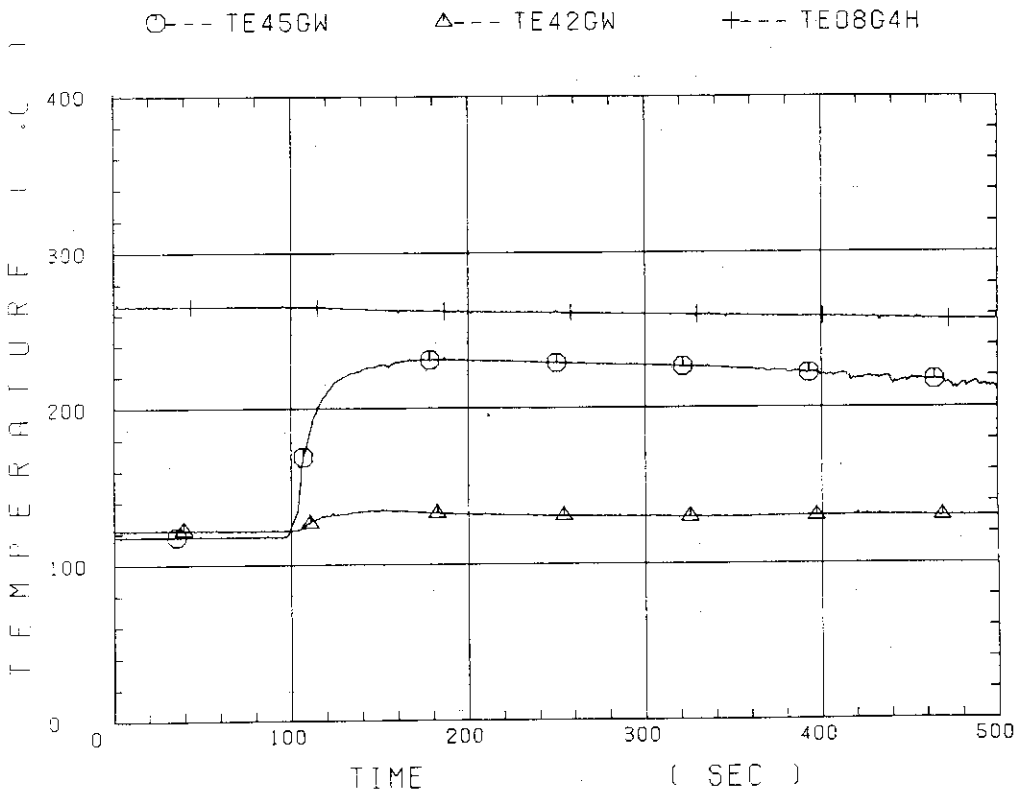


Fig. B-33 Fluid temperature in inlet plenum, output plenum, and secondary of steam generator 2

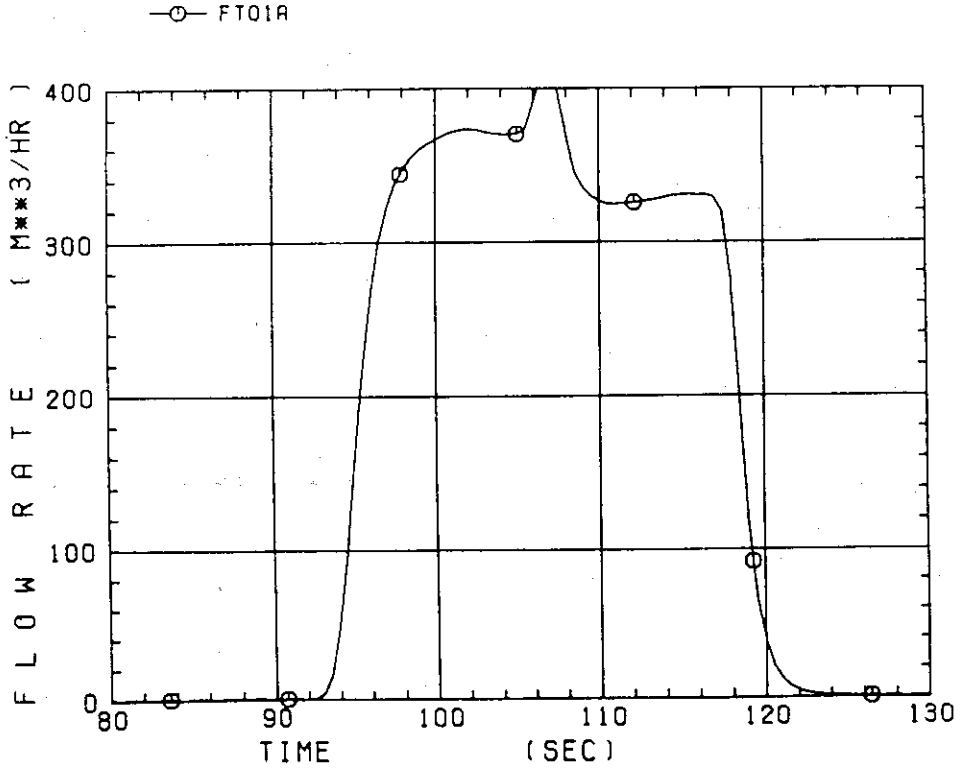


Fig. B-34 Total accumulator injection rate

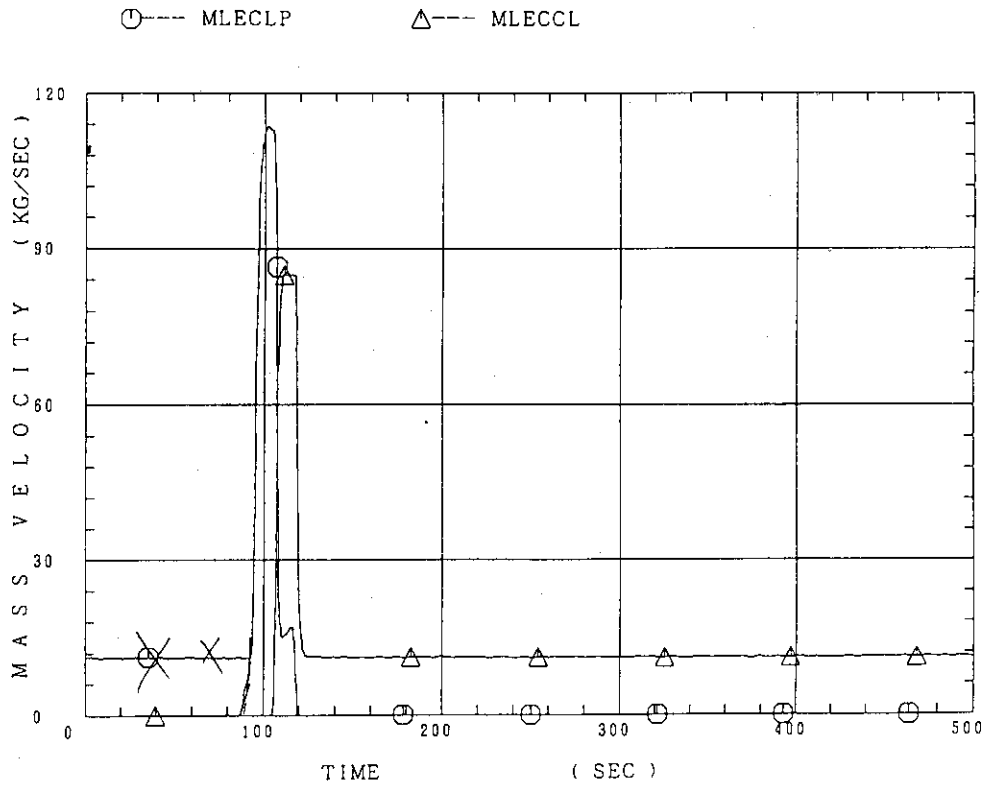


Fig. B-35 ECC water injection rates to lower plenum and to cold legs

# Appendix C

## Evaluation of core flooding mass flow rate

Figure list

The reflood phenomena is a relatively slow transient and is assumed to be a steady state condition. In a steady state condition, based on the mass balance relations of the system, the core flooding mass flow rates $\dot{m}_F$s can be written as follows:

By using the data measured at the downstream of the core inlet, $\dot{m}_F$ is derived as,

$$\dot{m}_F = \dot{m}_C + \dot{m}_U + \dot{m}_B + \Sigma \dot{m}_I \quad , \tag{1}$$

where $\dot{m}_C$ and $\dot{m}_U$ are the mass accumulation rates in the core and the upper plenum respectively. The $\dot{m}_B$ and $\dot{m}_I$ are the mass flow rates in the broken loop and the intact loop, respectively.

By using the data measured at the upstream of the core inlet, $\dot{m}_F$ is derived as,

$$\dot{m}_F = \Sigma \dot{m}_{DL} - \dot{m}_D - \dot{m}_O + \dot{m}_{ECC/LP} \quad , \tag{2}$$

where $\dot{m}_{DL}$, $\dot{m}_O$ and $\dot{m}_{ECC/LP}$ are the mass flow rates of the water flowing into and overflowing from the downcomer and the mass flow rate of the ECC water injected into the lower plenum, respectively.

The $\dot{m}_I$s AND $\dot{m}_B$ can be obtained from the pressure drops at the pump simulators with orifices by assuming the K-factor of the orifice is constant or from the data of Pitot tubes. The values of $\dot{m}_C$, $\dot{m}_D$ and $\dot{m}_U$ can be evaluated with the differential pressure $\Delta P_C$, $\Delta P_D$ and $\Delta P_U$, respectively, as follows:

$$\dot{m}_n = d(\Delta P_n S_n/g)/dt \qquad (n : C, D, U) \quad , \tag{3}$$

where g is the gravitational acceleration and $S_n$ is the crosssectional area. The value of $\dot{m}_O$ can be obtained from the liquid level X in the Containment tank 1 as,

$$m_O = d(X\rho_\ell S_o)/dt, \tag{4}$$

where $\rho_\ell$ is the liquid density and $S_o$ is the cross sectional area of the containment tank.

The value of $\dot{m}_{DL}$ is obtained from the following mass and energy

balance relations at each ECC port under the assumption of thermal equilibrium:

$$\dot{m}_{DV} + \dot{m}_{DL} = \dot{m}_{ECC} + \dot{m}_{I} \quad , \tag{5}$$

$$(\dot{m}_{DV} + \dot{m}_{DL})i = \dot{m}_{ECC}i_{ECC} + \dot{m}_{I}i_{I} \quad , \tag{6}$$

$$\begin{aligned} &\text{if} \quad i_g \geq i \geq i_\ell \ , \quad (\dot{m}_{DV} + \dot{m}_{LD})i = \dot{m}_{DV}i_g + \dot{m}_{DL}i_\ell \\ &\text{if} \quad i > i_g \quad , \quad \dot{m}_{DL} = 0 \quad , \\ &\text{if} \quad i < i_\ell \quad , \quad \dot{m}_{DV} = 0 \quad , \end{aligned} \tag{7}$$

where i is enthalpy of fluid and $i_\ell$ and $i_g$ are enthalpies of liquid and steam at the saturation temperature, respectively.

The fluid temperatures can be measured with thermocouples immersed in the fluid and the enthalpies $i_I$, $i_{ECC}$ can be estimated.

Mass balance calculations were performed with Eqs. (1) and (2), since it was found that the water entering the steam generator was completely evaporated. In the differentiation, higher frequency components of the data tends to be amplified more. Therefore, in the differentiation of the differential pressure data, the smoothing procedure was used to suppress the high frequency components of the data. Figure C-1 shows the flooding mass flow rates, $\dot{m}_F$s, calculated from Eqs. (1) and (2) by averaging data in 20 seconds.

In the Acc injection period, the calculated values $\dot{m}_F$s, are significantly different from each other. This discrepancy may be caused by inaccuracy of the mass flow rate injected into the system and by the unaccounting of the storage of water in the cold leg pipe. The former might be introduced from the slow time response (time constant 1 second) and the change of the gas volume in the injection line. In this period, specially before the steam generation from the core became noticable, the mass flow rate, $\dot{m}_F$, calculated with Eq. (1) is reasonable, since the calculation needs the increasing rates of the masses in the core and the upper plenum and their accuracy is enough for our estimation.

In the LPCI injection period, the calculated values, $\dot{m}_F$s, are slightly different from each other. Judging from the time-integral values of both $\dot{m}_F$s, their average values are nearly proportional. The discrepancy was inferred to be caused by the disregard of the bypass of steam and liquid from the upper plenum wighout going through the hot legs in the calculation with Eq. (1). And additionally the discrepancy was caused by the disregard of the steam generation in the downcomer due to the hot wall of the pressure vessel in the calculation with Eq. (2). It was estimated that the disregard of the downcomer steam generation was caused the error of 0.25 kg/s on predicted $\dot{m}_F$. The estimation was made by comparing the results of the tests with hot and cold downcomer conditions. In the LPCI injection period except for the early period, the mass flow rate, $\dot{m}_F$, calculated with Eq. (2) is reasonable, since the error from the injected ECC flow rate measurement is negligible under the quasi-steady state condition appeared in this period and the error caused by the steam generation in the downcomer is small.

In order to obtain the best estimate core inlet mass flow rate, the calculation with Eq. (1) were performed by using the corrected values of the loop mass flow rates, $\dot{m}_I$s and $\dot{m}_B$. The correction was made by multiplying $\dot{m}_I$s and $\dot{m}_B$ by a factor which yields identical $\dot{m}_F$s in the calculations with Eqs. (1) and (2). Figure C-2 shows the best estimate core inlet mass flow rate. In this calculation, the smoothing procedure was performed by averaging $\dot{m}_F$ in 10 seconds. Therefore the core inlet velocity at the reflood initiation was slightly lowered. Since the bypass of steam and water from the upper plenum is difficult to be evaluated quantitatively, this estimation involves at greatest about 15 % error. The relation between the integral core-flooded water mass evaluated with Eqs. (1) and (2) and best-estimated are shown in Fig. C-3.

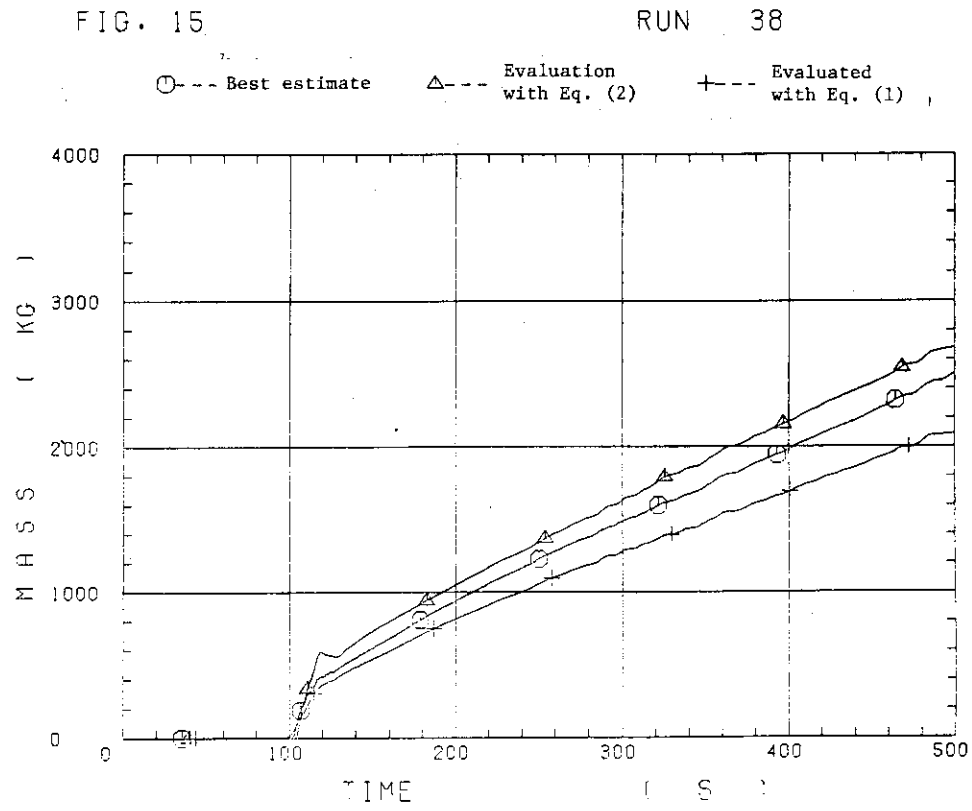


Fig. C-1 Core flooding mass flow rates evaluated with Eqs. (1) and (2)

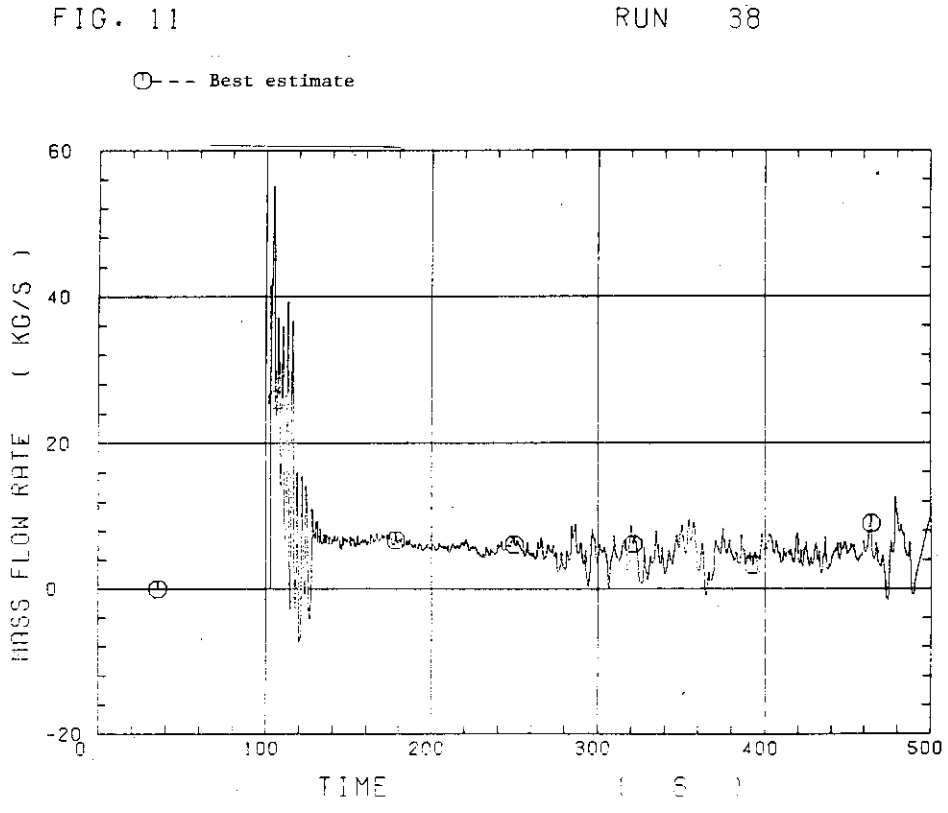


Fig. C-2 Best estimate core flooding mass flow rates

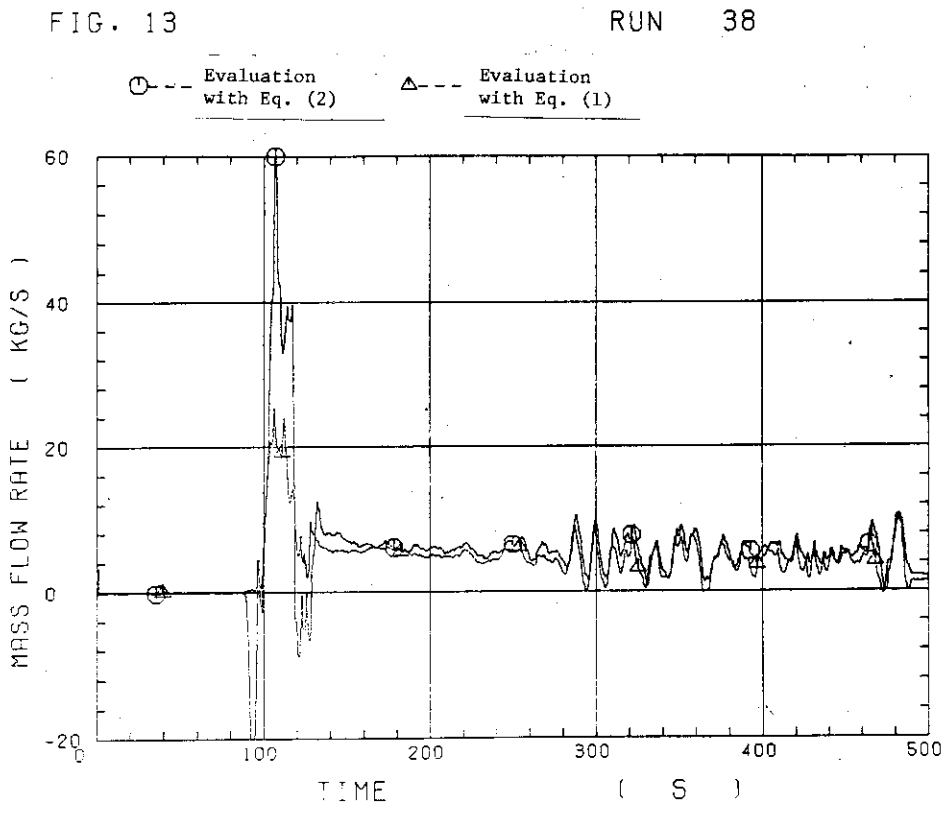


Fig. C-3 Integral masses flooded into core evaluated with Eqs. (1) and (2) and best-estimated